PERMEABILITY OF INTACT AND FRACTURED INDIANA LIMESTONE

Patrick Mattar

November, 2009

Department of Civil Engineering and Applied Mechanics
McGill University, Montréal
Quebec, Canada, H3A 2K6

A thesis submitted to McGill University in partial fulfillment of the requirements of the degree of Master of Engineering

Abstract

This thesis presents the laboratory techniques that were used to determine the permeability of intact and fractured Indiana Limestone. The cylindrical samples used in the experiments measured 100mm in diameter and 200mm in height with concentric axial cylindrical cavities of 23mm diameter along the entire length of the specimen. The permeability of the intact samples was determined by subjecting the sample to radial water flow until the inner pressure of the water-filled cavity reached a steady state. 6 to 18 tests were performed on each sample using different flow rates to obtain an average value of the permeability for each intact specimen of Indiana Limestone. The permeability of the intact specimens ranged from 0.9×10^{-15} m^2 to 1.9×10^{-15} m^2. A flat fracture perpendicular to the axis of the cylindrical samples was introduced; the change of the permeability of the fractured samples with quasi-cycled axial loading was determined. The same steady state constant flow test was used and the change in fracture aperture size was recorded. An initial increase in permeability of around 5 orders of magnitude was observed at the beginning of the first loading cycle and significant irreversible reductions of the fracture permeability were observed after each cycle. The fractures were finally sealed with anchoring gel epoxy and the permeability of the sealed samples was compared with those values for the intact samples.

Résumé

Cette thèse présente les techniques expérimentales utilisées pour déterminer la perméabilité du Calcaire d'Indiana en état intact ainsi que fracturé. Des échantillons cylindriques de 200mm de longueur et de 100mm de diamètre avec des cavités concentrique axiales cylindriques de 23mm de diamètre étaient utilisés. La perméabilité des échantillons intacts a été déterminée en appliquant un écoulement d'eau radial à travers les spécimens jusqu'à l'obtention d'une pression de cavité interne constante. 6 à 18 tests ont été effectués sur chaque échantillon en utilisant plusieurs débits pour obtenir une valeur moyenne pour la perméabilité de chaque échantillon de Calcaire d'Indiana. La perméabilité des spécimens intacts obtenue s'étend entre 0.9×10^{-15} m^2 et 1.9×10^{-15} m^2. Une fracture perpendiculaire à l'axe des spécimens cylindriques a été introduite et le changement de la perméabilité à cause d'efforts quasi-cycliques a été déterminé. Le même genre d'expériences (débit constant) utilisé avec les échantillons intacts a été utilisé avec les échantillons fracturés et le changement de la taille des fractures a été enregistré aussi. La perméabilité des spécimens fracturés augmenta d'environ 5 ordres de magnitude au début du premier cycle d'effort appliqué et une chute irréversible de la perméabilité des fractures a été remarquée à la suite de chaque cycle. Finalement, les fractures ont été scellées avec de l'époxy pour ancrage et la perméabilité des échantillons "intacts" a été comparée avec la perméabilité initialement obtenue des échantillons de Calcaire d'Indiana.

Acknowledgements

The work presented in this thesis was only possible with the suggestions, guidance, encouragement, and knowledge of the author's thesis supervisor Professor A.P.S. Selvadurai *William Scott Professor* and *James McGill Professor*, Department of Civil Engineering and Applied Mechanics, McGill University.

The author would like to express his gratitude to the technical staff at the Civil Engineering and Applied Mechanics Department at McGill University. The permeameter used in this research was conceptualized, designed and tested by Mr. P.A. Selvadurai. This device was essential to the research reported in the thesis. The author gratefully acknowledges this contribution. The test frame was designed by Mr. A. Chevrier of Carleton University. Mr. Damon Kiperchuk performed the preparation of the Indiana Limestone samples, Mr. Marek Przykoski assisted in the setup of the instrumentation and Mr. John Bartczak assisted in the design and construction of the water reservoir, the post-fracturing assembly and other fixtures.

The author would like to thank his colleagues: Dr. Hani Ghiabi, Mr. Tuan Anh Luu, Mr. Antoine Letendre, Mr. Kevin Fournier, Dr. Alex Suvorov and Miss. Mei-Qiong Shi for their advice, encouragement and moral support.

The author would like to express appreciation for the Computer Science Artificial Intelligence unit at McGill University, mainly PhD candidate Amin Atrash for his assistance in writing a Matlab code that was essential for data acquisition.

The author would like to thank Mrs. Sally Selvadurai for correcting an initial draft of the thesis.

The research work was made possible by an NSERC Discovery Grant awarded to Professor A.P.S. Selvadurai.

Finally, the author would like to express his eternal appreciation for the support of all his friends and his family.

Table of Contents

List of Tables

List of Figures

<u>Paper Resulting from the Research</u>

Conference Publication

Mattar, P. and Selvadurai, A.P.S. (2009) Radial Flow Permeability Testing of Indiana Limestone, *Proceedings of the 3rd CANUS Rock Mechanics Symposium, May 2009,* (Ed: M.Diederichs and G.Grasselli), Toronto, Ontario, pp. Paper-4119: 1-7.

Chapter 1 - Introduction

The study of fluid flow through soils and rocks is particularly important when dealing with groundwater movement in surficial geomaterials that can be initiated by hydraulic gradients developed during construction activity, groundwater extraction, impounding of reservoirs and groundwater recharge during adverse climatic events. In a geotechnical context, intact rocks are regarded as virtually impermeable materials, with comparatively greater resistance to flow of water through their pore structure. In contrast, fluid transport in fractured rock masses is largely governed by the permeability of the apertures. In conventional hydrogeological applications, the fracture permeability is usually assumed to be an unchanging property, determined from in situ tests, involving either steady state or transient tests. When the geostatic stress field changes as a result of engineering activities such as underground excavations, groundwater lowering, etc., fractures can experience closure or widening and this can result in an alteration in the fluid transport characteristics.

The permeability of rocks and fractured rocks is important when deep geologic formations are to be used in geo-environmental activities for disposal of hazardous and toxic materials, since the movement or transport of the hazardous materials during their eventual release will be largely governed by the permeability characteristics of the geologic formation (Mattar and Selvadurai, 2009). The estimation of the permeability characteristics of geologic formations is a non-trivial exercise since the measure of permeability can be influenced by the scale at which the measurement is made.

The intact and fractured permeability of geomaterials is regarded as an important property that influences the efficiency and reliability of engineering solutions for deep geologic disposal. The in situ permeability characteristics of intact rocks have been examined since the construction of concrete dams founded on rock (Mayer, 1963; Stagg and ZienZiewicz, 1968; Jaeger, 1972). Laboratory permeability measurements of relatively low permeability geomaterials, including rocks and concrete, has been the subject of extensive research over the past four decades; the testing methods include both steady state flow and pressure transient techniques conducted on cylindrical cores of rock. Ideally, the simplest technique for determining the permeability of intact rock involves the attainment of steady state flow or steady state pressure conditions in a sample, which is both easy to perform and easy to analyze theoretically (Daw, 1971; Heystee and Roegiers, 1981; Morrow and Byerlee, 1988; Lockner et al., 1991; Song et al., 2004; Selvadurai and Selvadurai, 2007; Selvadurai and Glowacki, 2008).

This thesis presents the results of an experimental investigation that examines the permeability of intact Indiana Limestone, the effect of quasi-cycled stresses on the permeability of fractured Indiana Limestone and finally, the permeability of sealed fractures in Indiana Limestone. The permeability of intact Indiana Limestone was obtained using the steady state constant flow technique which involves establishing a steady state radial flow in a cylindrical sample of Indiana Limestone; the resulting stabilized water pressure in the cavity of the sample is used to determine the permeability of the limestone. The radial flow permeability test is not a straightforward test for determining the permeability of geologic materials since the experimental configuration should assure that the seals enabling the application of a constant radial flow are effective and do not allow leakage that would give erroneous estimations of the permeability. A flat fracture, normal to the axis of the cylindrical sample is induced; the fractured sample is re-assembled, making sure the fractured plane is free of rock debris. The permeability of the fractured samples was determined using the steady state constant flow test as well while subjecting the sample to different axial stresses. The permeability of the fracture is evaluated at every stress level using the model of the flow of a viscous fluid through a set of parallel plates. The experimental results show a hysteresis effect in the evolution of permeability with stress. Finally, the fractured samples were sealed using epoxy anchoring gel and the steady state constant flow technique was used to determine the permeability of the remediated samples.

Chapter 2 - Literature Review

This chapter presents a literature review of the laboratory methods used to determine the permeability of rocks which include steady state and transient tests as well as in-situ tests. The advantages and disadvantages of each method are discussed. Documented permeability results of Indiana Limestone, the rock used in this research, are summarized. The permeability of fractures in rocks is also presented. Details of the experimental configurations, the samples used and the results obtained are also summarized.

2.1 - Laboratory Methods for Determining the Permeability of Rocks

Laboratory techniques are one option for determining the permeability of rocks. The relatively small size of the samples chosen for a laboratory test minimizes dramatically the possible occurrence of discontinuities or inhomogeneities. Another obvious advantage of laboratory testing is the ability to control the environment affecting the properties of the sample and the fluid. The two most popular categories of laboratory testing are steady state tests and transient tests.

Steady state tests (Figure 2.1-a) involve the application of a fluid pressure gradient across a sample which will eventually result in a steady flow rate that is used to calculate the permeability. The experimental setup for a steady state test requires a permeameter that supplies water to the sample, a system that provides a constant hydraulic head across the sample, and a device to measure the resulting flow rate that will eventually reach steady state. The "permeability cell" described by Daw (1971), based on an original design by Hoek and Franklin (1967) is one of the earliest examples of the steady state constant head technique applied to rocks. The modified cell is a triaxial cell that allows the testing of rock cylinders of diameter 25.4mm and length 25.4mm. The apparatus allows axial fluid flow through the sample, with a seal provided on the sides of the specimens using rubber membranes, which were compressed. Daw (1971) indicates that the sealing pressure required to provide a good seal should be 20% greater than the maximum fluid pressure applied. He advised that larger sealing pressures reaching twice the maximum pressure applied should be used.

The other variant of steady state testing (Figure 2.1-b) that is commonly used involves the application of a constant flow rate across the sample, which will eventually result in a steady state water pressure used for the calculation of the permeability coefficient. The experimental configuration is quite similar to the constant head configuration, where the same permeameter can be used but the constant head provider is replaced by a constant flow provider, typically a pump; the device used to measure flow rates is replaced by a pressure transducer which measures the water pressure until it reaches steady state. The flow pump method used by Olsen (1966) and revised by Olsen et al. (1985), is a direct application of the constant flow test. In the latter study, it was used to test the permeability of sand, sandy silt, and silty clay but the method can theoretically be applied for rocks as well (Carnaffan, 1994).

The two steady state techniques discussed above (Figure 2.1) are used on rocks such as limestone and sandstone which generally tend to have permeabilities in the range of $1.5\times10^{-10}m^2$ to $4.4\times10^{-16}m^2$ (Selvadurai and Selvadurai, 2007; Selvadurai and Glowacki, 2008). With low permeability rocks, such as dense limestone, granite, concrete, cement grout etc, with permeabilities in the range of $10^{-19}m^2$ to $10^{-22}m^2$, large fluid pressure gradients are needed to initiate steady flow rates. This requires adequate sealing techniques which can only be provided by subjecting the sample to large confining stresses and sealing loads. These large pressures and loads can influence the permeability of the tested rock by expanding micro-cracks and other fissures.

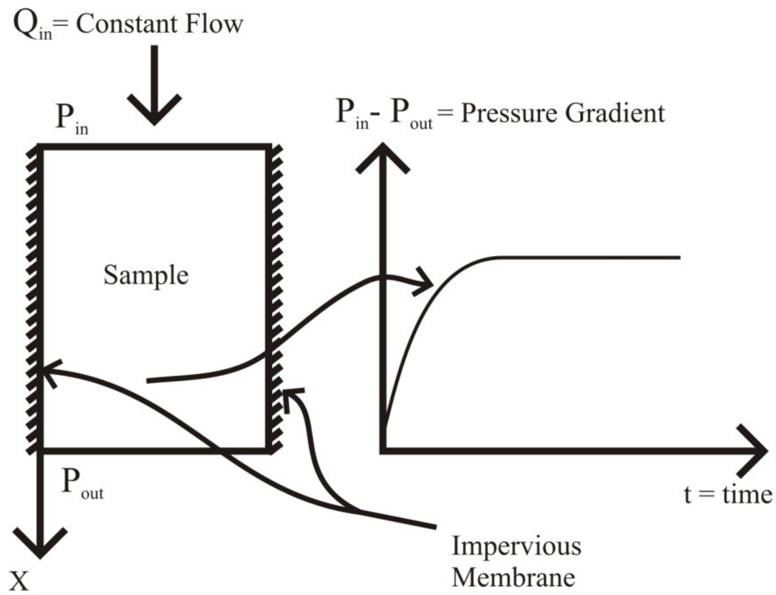

(a) Steady State Constant Flow Test

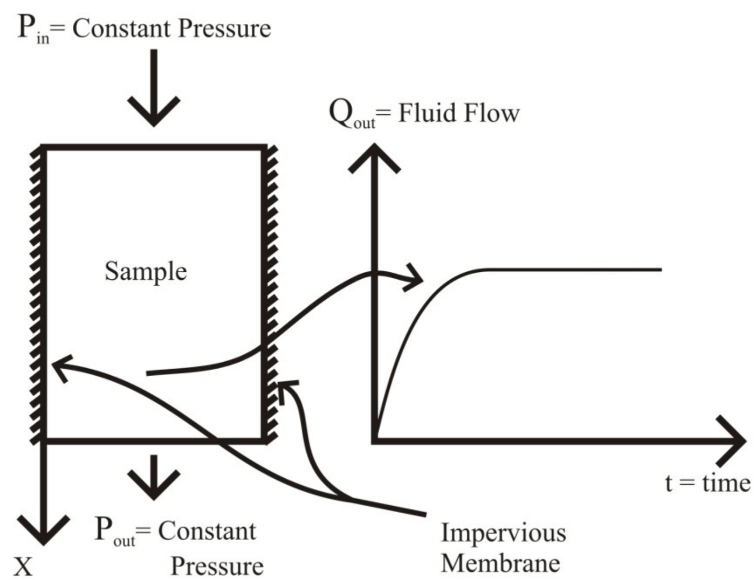

(b) Steady State Constant Head Test

Figure 2.1 - Steady State Permeability Tests

Transient permeability testing (Figure 2.3) is suitable for geomaterials that have a low permeability ($10^{-19}m^2$ to $10^{-22}m^2$). The most popular of the transient methods is the pulse decay method (Figure 2.3–a), where the tested sample is confined and arranged in such a way that it can be connected to an upstream and a downstream reservoir. This system, consisting of the sample and the two reservoirs, is initially pressurized requiring pressure transducers and pressure supply sources. The basic method involves the application of an incremental pressure in the upstream reservoir which eventually results in a gradual decay of pressure in the upstream reservoir and a gradual increase in pressure in the downstream reservoir until a new equilibrium pressure in the system is reached. These measured pressures are recorded over time allowing for the determination of the permeability coefficient.

Brace et al. (1968) presented one of the first papers where the pulse decay method is used. The samples tested were cylinders of Westerly Granite 16.1mm in height and 25.2mm in diameter. The samples were confined to effective pressures ranging from 10MPa to 400MPa, which gave permeability values ranging from $350\times10^{-21}m^2$ to $4\times10^{-21}m^2$. The paper itself gives a graph with typical values of the initial pressure in the system (40MPa), the incremented pressure (2MPa), and the change of the pressure in the upstream and downstream reservoir with time.

Bernabe et al. (1982) tested the permeability of hot pressed calcite samples, 12.5mm in diameter and 5 to 15mm in length using the steady state approach as well as the transient pulse decay approach. In the transient tests, the experimental configuration was inspired by Brace's original design (Brace et al., 1968). Pulses of around 5 to 10% of the fluid pressure were generated in the upstream reservoir and the differential decay in pressure recorded. The ambient temperature was controlled and this was an improvement on the earlier research of Brace et al. (1968). The accuracy of the system was checked by applying steady state and pulse decay methods on 4 hot-pressed quartz samples and the results were consistent up to within 10%. The samples of hot pressed calcite had different porosities; and it was noted that the permeability drastically decreased with a decrease in the porosity. These results helped in understanding the pore geometry changes in the calcite during the hot pressing process.

Bernabe (1986) described the use of the pulse decay technique on cores of two types of granite (Chelmsford and Barre). The Chelmsford coring orientation was critical and lead to the preparation of one sample for each orientation (i.e. perpendicular to Rift, Grain, and Hardway planes) (Figure 2.2). Several Barre Granite samples were prepared from a non-oriented core. These cylindrical samples were 19mm in diameter and 25mm in height and the dimensions were controlled by the experimental arrangements. Special attention was given to the cut faces so that they were either parallel or perpendicular to the axis of the cylinders. The samples were also saturated by immersion in distilled water under vacuum. A 20% change in permeability was observed in the Chelmsford samples of different coring orientation and permeability decreased with increasing confining pressure. In Barre Granite, a 15% difference in permeability was observed between the two samples, with a notable hysteresis effect especially after the first loading cycle.

A slightly different type of transient permeability test (Figure 2.3-b) was described by Bourbie and Walls (1982). In this test the pressure was built-up by increasing the upstream reservoir pressure to a constant value (instead of releasing as in the conventional pulse decay method). A build up in pressure consequently occurs in the downstream reservoir and the difference in the pressure between the reservoirs is measured. Nitrogen gas was applied to sandstone cylinders of diameter 50.8mm and length 67mm, using the pressure build-up method as well as the steady state method in order to compare between the permeability values obtained from the two techniques. It was found that the results obtained from the pulse decay method were valid.

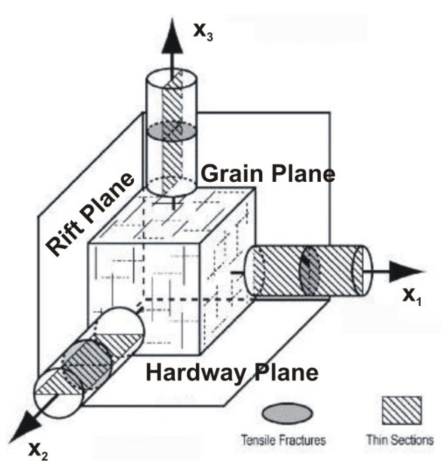

Figure 2.2 - Rift, Grain and Hardway Orientation Planes in Granite

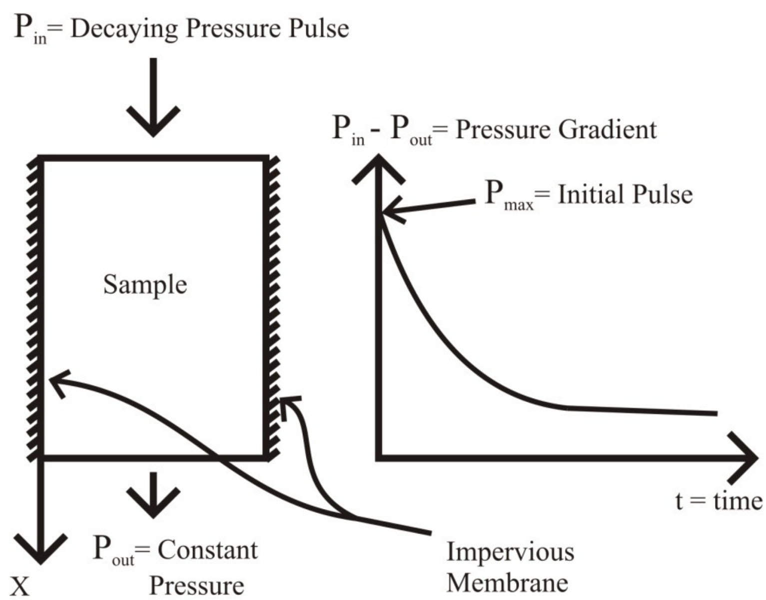

(a) Transient Pulse Decay Test

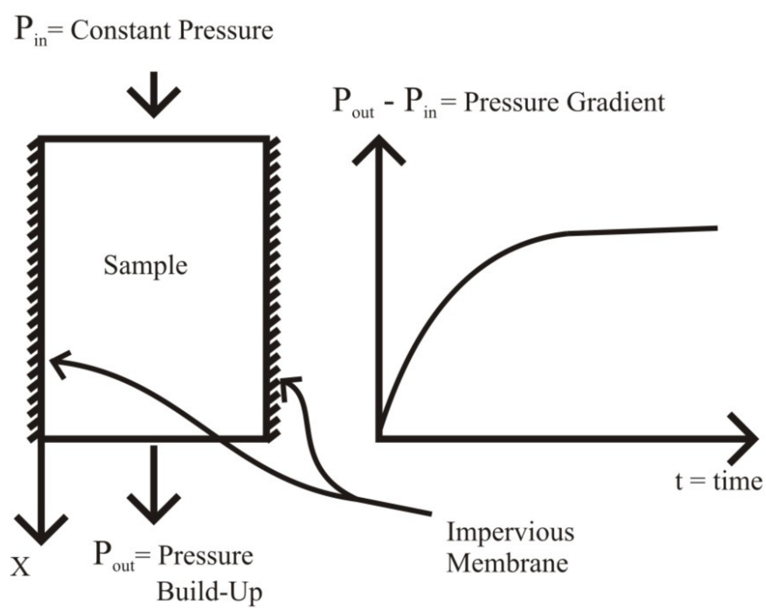

(b) Transient Pressure Build-Up Test

Figure 2.3 - Transient Permeability Tests

Reviews of the two main types of experimental techniques discussed above (the steady state and the transient) can be found in the articles by Selvadurai and Carnaffan (1997), Selvadurai et al. (2005) and Selvadurai (2009). The various advantages and disadvantages of the two basic approaches are fully discussed in these articles. Ideally, the simplest technique for determining the permeability of rocks involves the attainment of steady state flow conditions in a sample. This procedure can only be effective when the permeability of the material allows the attainment of the pressure gradient within an acceptable time frame. For simple one-dimensional steady flow conditions, the permeability can be estimated from the knowledge of the hydraulic gradient and the dimensions of the sample or the flow domain. In transient tests on the other hand, in addition to the above data, information should also be available on the compressibilities of the pore fluid and porous fabric as well as the porosity of the medium. Unless these parameters can be determined *a priori*, the accurate interpretation of the transient permeability tests is not feasible. The main advantage of the transient test is that it can be performed relatively quickly whereas the steady state tests require time to establish a steady state. The choice of the most appropriate test ultimately depends on the type of material that is being examined. Transient tests are advocated for rocks such as granite (also cement grout) that has relatively low permeability ($10^{-19}m^2$ to $10^{-22}m^2$) (Brace et al., 1968; Selvadurai and Carnaffan, 1997; Selvadurai et al., 2005) while the steady state tests can be used for determining the permeability of materials with a comparatively high permeability, including sandstone and Indiana Limestone, the rock type used in this research ($10^{-10}m^2$ to $10^{-16}m^2$) (Selvadurai and Selvadurai, 2007; Selvadurai and Glowacki, 2008).

The laboratory methods described above (the steady state and the transient) can be used by supplying the fluid through the sample in a one-dimensional axial manner or in a radial manner such as in the experiments performed in this research. More complex flow patterns have also been used and these require computational analysis to evaluate the permeability coefficient.

The majority of laboratory permeability testing of rocks involves the percolation of fluids through the axial direction of cylindrical rock samples while confining the outer surface of the samples using impervious membranes; this is considered as the least invasive technique.

Morrow and Byerlee (1988) used the steady state constant head method on rock excavated from Cajon, California which is a major fault zone and source of earthquakes. The determination of the permeability of these rocks is important because it reflects the heat flow properties as well as quantifying the frictionally generated heat that is transported by groundwater to the fault zone. The samples of rock tested represented the different rock formations obtained from a 2100m borehole where the first 500m was occupied by sandstone underlain by crystalline rocks. The specimens were retrieved from the intact parts of this borehole. These samples were all machined to 25.4mm diameter and 25.4mm length cylinders. The samples were sealed with polyurethane tubing that was clamped on the outside to guide the flow along the axial direction of the cylinder. The differential pressure across the sample was held at 1MPa using a pressure intensifier. The flow rate of water was measured using the change of volume of the intensifier on the inlet side of the sample. Temperature was controlled and kept steady at 27°C. A period of 24 hours was required to reach steady state. The permeability results of 40 samples were reported. The large variations observed were due to two main reasons: First, the different levels of confining stress that were applied (each corresponding to the level of confining stress measured in-situ) to the different types of rock, and second, the variation in the coring orientation of the samples in order to test for the anisotropic properties of these rocks. These permeabilities were considered minimal rather than average due to the fact that the non tested parts of the borehole contained large amounts of cracks which would dramatically increase the permeability of the specimen.

Steady state constant flow permeability tests were performed by Lockner et al. (1991) on rock excavated from a depth of 11 to 12km in the Kola Peninsula in the former Soviet Union. The tested specimens were 3 intact cylindrical cores of diameter 25.4mm and lengths ranging from 13 to 24mm representing 3 types of rock present at this depth. Confining pressures ranging from 10MPa to 400MPa were applied to reflect the actual pressures at the depth where these rocks were extracted from. The material used to provide the confinement pressure seal was not mentioned. The resulting permeabilities ranged from $1\times10^{-17}m^2$ to $1\times10^{-22}m^2$. These permeabilities were considered upper bound values of the real in situ permeability due to the stress relief cracks that occurred during the excavation, leading to higher permeability values. The pressure relief cracks were distinguished from in-situ cracks by comparing the aperture size v/s effective pressure plots of surface cores and the deep Kola Peninsula cores.

Suri et al. (1997) performed oscillating pulse permeability tests on Indiana Limestone subjected to different stress paths in a triaxial cell. Steady state tests were also performed. The samples used were cored cylinders machined to a height to diameter ratio of at least 2. Vacuum was used to saturate the samples. The water flow was conveyed through the axial direction of the samples using porous plates to uniform pore pressure between the upstream and downstream ends of the sample. The confining pressure provided in the triaxial cell was prevented from interfering with the system by Teflon jacketing the outer surface of the specimens. Results of the different tests performed (hydrostatic compression tests, triaxial compression tests, uni-axial strain tests) and the corresponding variation that occurred were discussed in the paper.

An experimental configuration combining steady state and transient concepts to determine permeability and specific storage simultaneously is discussed by Song et al. (2004). Cylindrical samples of Westerly Granite, measuring 38mm in diameter and 40mm in length, were used to demonstrate the efficiency of the experimental methodology. These samples were first vacuum saturated for 24hrs and confined using a rubber jacket to 35kPa throughout the experiments. Water was therefore forced to flow through the cylindrical direction of the sample and the outlet pressure was measured using a transducer. The measured permeabilities ranged from $3.5\times10^{-19}m^2$ to $3.6\times10^{-19}m^2$. Song and Renner (2006) also used this technique on Fontainebleau Sandstone samples and obtained a permeability of $3.5\times10^{-16}m^2$.

Selvadurai and Glowacki (2008) applied incremental confining pressures and axial loads on cylindrical limestone samples measuring 100mm in diameter and 200mm in height, while a constant flow rate was applied along the axial direction. The maximum confining pressure applied was 60MPa. The pressures were applied using a GDS Triaxial testing facility and the details are presented by Selvadurai and Glowacki (2008). The membrane chosen to provide a seal that could handle large pressures without rupturing was a close-fitting nitrile rubber of 2mm thickness with an un-stretched internal diameter of 91 mm. The aim of the research was to obtain the permeability hysteresis for the Indiana limestone under different isotropic confining pressures. After 272 steady state constant flow rate tests, the results clearly show a decrease in the permeability with an increase in confining pressure as well as irreversible changes in permeability after the application of certain confining pressures.

In recent years, researchers testing rock permeability by fluid permeation have often opted for radial flow tests (Figure 2.4). The general experimental configuration for radial flow experimental testing is similar to the axial flow configuration for steady state or transient techniques. Other than the risk of the alteration in the hydraulic properties of the sample due to the invasive process of creating the cavity, the main difference between the two techniques is that the radial flow test does not require a confining seal around the outer surface of the sample. However, a good seal (usually vacuum-greased rubber O-rings) should be provided at the two smooth parallel sides (upper and lower) of the cylinder around the cavities, blocking one cavity end with an impermeable material (such as stainless steel) and applying the fluid from the other end allows the fluid to seep through the unconfined outer surface of the tested sample.

Londe and Sabarly (1966) examined the variation in permeability of rock specimens with applied stresses. The rock was extracted from the foundation of an arch dam and is characterized by micro-fissures dispersed in the rock matrix that are the main routes for percolating fluids. The study performed is one of the earliest to involve converging and diverging radial flow percolation through cylindrical samples with a drilled cylindrical cavity.

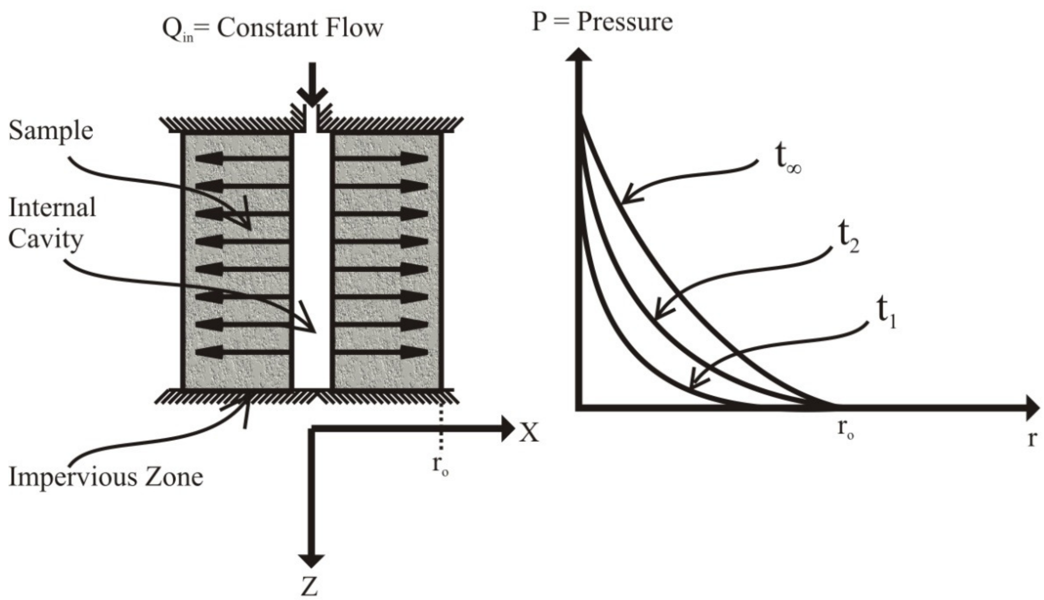

Figure 2.4 - Steady State Radial Flow Test

Jaeger (1972) discusses two types of radial percolation tests performed by the Ecole Poly-technique Laboratory (Paris, France), where the first involves radial convergent flow and the second radial divergent flow. The theoretical procedure to determine the permeability is based on Darcy's Law and was shown to be the same for convergent and divergent flow. Some of the tests performed in the Ecole Poly-technique Laboratory (Paris, France) on St-Vaast Limestone show the same results for both radial direction tests. A noticeable difference between convergent and divergent radial percolation tests is the fact that the internal stresses during fluid percolation are compressive during the first and tensile during the second. For that reason, the flow rates and consequently the pressures induced in the system should be limited to the tensile strength of the tested rock. As a comparative conclusion between classical longitudinal percolation tests and radial percolation tests performed in the Ecole Poly-technique Laboratory (Paris, France), Jaeger (1972) comments on the advantages and disadvantages of the two tests. First, radial permeability tests are more informative when samples are subjected to varying strains with the only drawback being that they are time consuming. Second, longitudinal percolation tests are inapplicable to very impervious rocks.

The permeability properties of three types of rock were examined by Heystee and Roegiers (1981) since permeability affects fluid penetration, an essential factor in hydraulic fracturing processes. The samples tested were Indiana Limestone, granite (red and coarse grained) and Red Sandstone cylinders measuring 64mm diameter and 100mm in length. The steady state constant head method was used with flow applied through a 6.4mm in diameter and 87mm length drilled cavity. Epoxy resin was used to seal the top and bottom surfaces of the cylinders. For divergent radial flow, a tube fitting was epoxy-glued at the exposed cavity end. The divergent flow tests investigated the effect of tensile stresses on the hydraulic property of the tested material. Convergent radial flow tests were also performed to investigate the effect of compression stresses on the coefficient of permeability.

Selvadurai and Carnaffan (1997) used transient pressure pulse techniques to test the hydraulic properties of very low permeability cementitious grout. It was observed by the authors that there were no Canadian Standards Association (CSA) or American Society for Testing and Materials (ASTM) standardized laboratory tests, for measuring the permeability of concrete using the radial flow pulse test. With the goal of having such a standardized test, the following experimental setup and methodology was proposed: Grout cylinders 225mm in length and 152mm in diameter with a central cavity of 26mm diameters, were first vacuum saturated with water. A pressure transducer was located in the water at the base of the central cavity and an axial load of 5kN was provided to a stainless steel plate, which created a seal at the upper side of the cavity as well as housing the water connections for injecting fluid to the cavity. The entire sample was placed in a reservoir. Further details of the experimental setup can be found in the paper. Selvadurai and Carnaffan (1997) outlined the advantages of using their experimental facilities over the original one proposed by Brace et al. (1968); firstly, the improved setup is simpler and no confining seal had to be provided at the outer surface of the cylinders. Second, the only load required is an axial load to seal the cavity. Finally, the placement of the pressure transducer in the central cavity allows for more accurate measurements.

Selvadurai et al. (2005) conducted radial flow permeability tests on a cylindrical Barre Granite sample, 457mm in diameter and 510mm in height, containing a cylindrical cavity of diameter 51mm. First the sample was subjected to a high axial load, which was necessary to provide a seal between the sample and the O-rings placed on both plane ends of the sample. The hole was then filled with de-aired water. A supply pump was used to provide a flow rate and a pressure in the sample cavity. Permeability was thus measured for the unsaturated sample. Following the saturation of the sample by applying a small flow rate of de-aired water for 288 hours, permeability was again calculated. In the test itself, the decay of the water pressure in the cavity was recorded every 2 seconds. Finally, the sample was heated before testing to study what effect this had on the properties of the granite, mainly the permeability property. Further details of the theory behind permeability calculation after heating can be found in Selvadurai et al. (2005), where the transient flow problem from a cylindrical cavity, which is governed by Darcy's law, is described.

Axial flow as well as convergent and divergent radial flow measurements were performed by Areias and Lo (2006) to determine the hydraulic conductivity of rocks extracted from a 390m deep borehole in Lakeview, Southern Ontario, Canada. Lindsay Limestone and Verulam Limestone were found in the cores. First, axial flow permeability testing was performed in a triaxial cell on samples of 45mm in diameter and 15mm to 20mm in length. In these experiments the outer surface of the rock discs was sealed using a layer of grease to separate the specimen from an impervious rubber membrane. The rock specimens used for testing radial flow permeability were 45mm in diameter and 112mm in length. A cavity of 11.2mm in diameter was drilled from the top flat face to 20mm above the bottom face along the axial direction of the cylindrical samples. The sample preparation included a coating of acrylic compounds around the circumferential area of the cylinder at the bottom 20mm and the top 17mm and then covering this with impervious rubber sleeves. This configuration created dead flow zones at the ends of the specimens, which created the desired axi-symmetric radial flow condition. Axially loaded O-rings were used to create a seal at the top water inlet location. Convergent and divergent radial flow conditions were created by shifting the differential pressure between the triaxial cell and the pressure in the central hole. The hydraulic conductivities obtained from axial flow tests ranged from 1.1×10^{-14}m/sec to 3.8×10^{-11}m/sec. The hydraulic conductivities obtained from radial flow tests ranged from 1.9×10^{-14}m/sec to $8.2\times10^{-}$

^{12}m/sec. The results from both tests were compared to examine anisotropic features of the rock; one sample showed a large difference in the hydraulic permeability values obtained from radial and axial flow tests.

As seen from the above discussion, the samples used to test permeability in the radial direction are usually cylindrical in shape. In some cases though (Lafhaj et al., 2007; Selvadurai and Selvadurai, 2007), cuboidal blocks with cylindrical cavities have also been used.

Lafhaj et al. (2007) presented a non-conventional, non-destructive technique to measure permeability of rock in-situ. Air was used as the permeating fluid through a drilled hole in the rock. The dimensions of the cavity should be minimal compared to the sample size; thus, this technique is considered to be non-destructive and can be used on natural rock found in-situ or with concrete. The samples tested were two blocks of Anstrude Limestone and concrete respectively, of 500mm width and 150mm height. Several holes were drilled at different locations, 14mm in diameter and 50mm in depth. The flat bottoms of the cavities were covered by a special plug system that would only leave the inner circumferential area of the cavity exposed to air. Permeability was estimated by creating a vacuum in the cavity causing convergent air flow through the tested rock into the hole and then measuring the evolution of pressure with time. The permeabilities of Anstrude Limestone obtained ranged from 1.3×10^{-16}m^2 to 1.8×10^{-16}m^2. The validity of this in-situ testing apparatus was confirmed by comparing the results with laboratory test results performed on cylindrical samples of the same rock type. The difference between the two sets of results was deemed acceptable.

In the experiments performed by Selvadurai and Selvadurai (2007) a constant water flow rate was maintained by pressurizing a central cavity drilled into a large sandstone block to determine its bulk permeability. The block was 450mm^2 in plan area and 508mm in height, which is considered large enough to take into consideration the inhomogeneities of geologic media (i.e. fractures, fissures, inclusions, etc.) that might not be possible when testing smaller cylindrical samples. The central cavity had a diameter of 63.5mm. All radial flow permeability testing systems need to pay special attention to the sealing of the top and bottom faces of the block; in this case epoxy resin was used. The cavity itself was sealed with axially loaded O-rings to form a no-flow zone beyond the lower end of the cavity and to prevent leakage from the water inlet zone at the top end of the cavity. The permeability of the sandstone block was determined experimentally using the configuration described above as well as computationally using a finite element model, details of which are discussed in the paper (Selvadurai and Selvadurai, 2007). The permeability of the block was estimated at $3.46\times10^{-15}m^2$ to $4.07\times10^{-15}m^2$.

Other experimental configurations have been used recently where no cavity is created in the sample and the flow is not one-directional. Tidwell and Wilson (1997) describe a laboratory method intended to investigate permeability upscaling in rocks. The need for such upscaling techniques stems from the fact that the permeability of porous media is usually determined on samples or locations that are not representative of the whole "un-sampled" site; an adequate upscaling technique is thus required. A multi-support gas permeameter, a device that can be adjusted to supply gas flow at different locations and at different flow rates, was used to convey compressed laboratory grade nitrogen at different locations of an intact sample. The specimen tested was a Berea Sandstone cubic block with side dimensions of 300mm. Special attention was paid to keeping the cube surfaces as flat as possible to allow an efficient seal. A special frame was built to supply a load to the permeameter and allow the permeameter to move to different locations. Permeability calculation was governed by the size of the seal used, the applied flow rate and the injection pressure. Results from 9 locations for each face were obtained and analyzed for the sandstone sample and others.

Selvadurai and Selvadurai (2009) developed an innovative non-invasive technique to determine surface permeability of rocks. A large cuboidal Indiana Limestone sample with 500mm sides was used for this experimental investigation. Constant water flow was conveyed to the sample through circular apertures created when sealing each test location with a special mechanism incorporated in the permeameter used. Steady state constant flow tests were performed on 9 locations of each face to obtain a distribution of the permeability across the limestone block. A computational model was used to interpret the data and project the surface permeability obtained to the interior of the sample. The results showed that the average permeability obtained for 2 faces were $29.4\times10^{-15}m^2$ and

$44.3\times10^{-15}m^2$. The wide range of permeability obtained from just two faces lead to the expectation that an even wider range of permeability might be encountered when all the faces are tested, indicating possible anisotropy in the sample.

2.2 - In-Situ Methods for Determining the Permeability of Rocks

In-situ testing of porous media is a common approach in geotechnical engineering, which provides estimates of the permeability coefficients of a specific site, and can include the influences of features such as fissures, fractures, anisotropy and non-homogeneities. These tests are thus only pertinent to the project planned for the region under investigation and do not provide information about the general hydraulic properties of the intact material, especially when the porous medium is a rock formation. Another important aspect of in-situ permeability testing methods is their applicability to low permeability formations such as rocks.

The packer test is the most commonly used field technique for testing the permeability of rocks. In the case of a known water level in an open hole, the packer test is preferred to other in-situ tests because it can be used to determine the hydraulic characteristics of the borehole at different levels which provides a better understanding of the vertical distribution of the rock at the specific site. Carnaffan (1994) gives a detailed description of the packer test (Figure 2.5) and its two variations (constant head test and pulse test). The test consists of drilling a hole in a specific site and applying a seal (provided by an inflatable packer) to a section above the base of the drillhole. Alternatively, a double packer (Figure 2.5-b) can be used where two packers provide a seal between two different levels of the borehole. The constant head test is performed by injecting fluid at a specified flow rate into the sealed area and recording the resulting constant head. The constant head in an observation well at a know distance from the drillhole is also recorded and the combined results are used to determine the hydraulic conductivity. The pulse test (Bredehoeft and Papadopulos, 1980) consists of applying a known pressure pulse the water-filled sealed part of the cavity and then allowing the cavity pressure to decay. This transient pressure decay is used to determine the permeability.

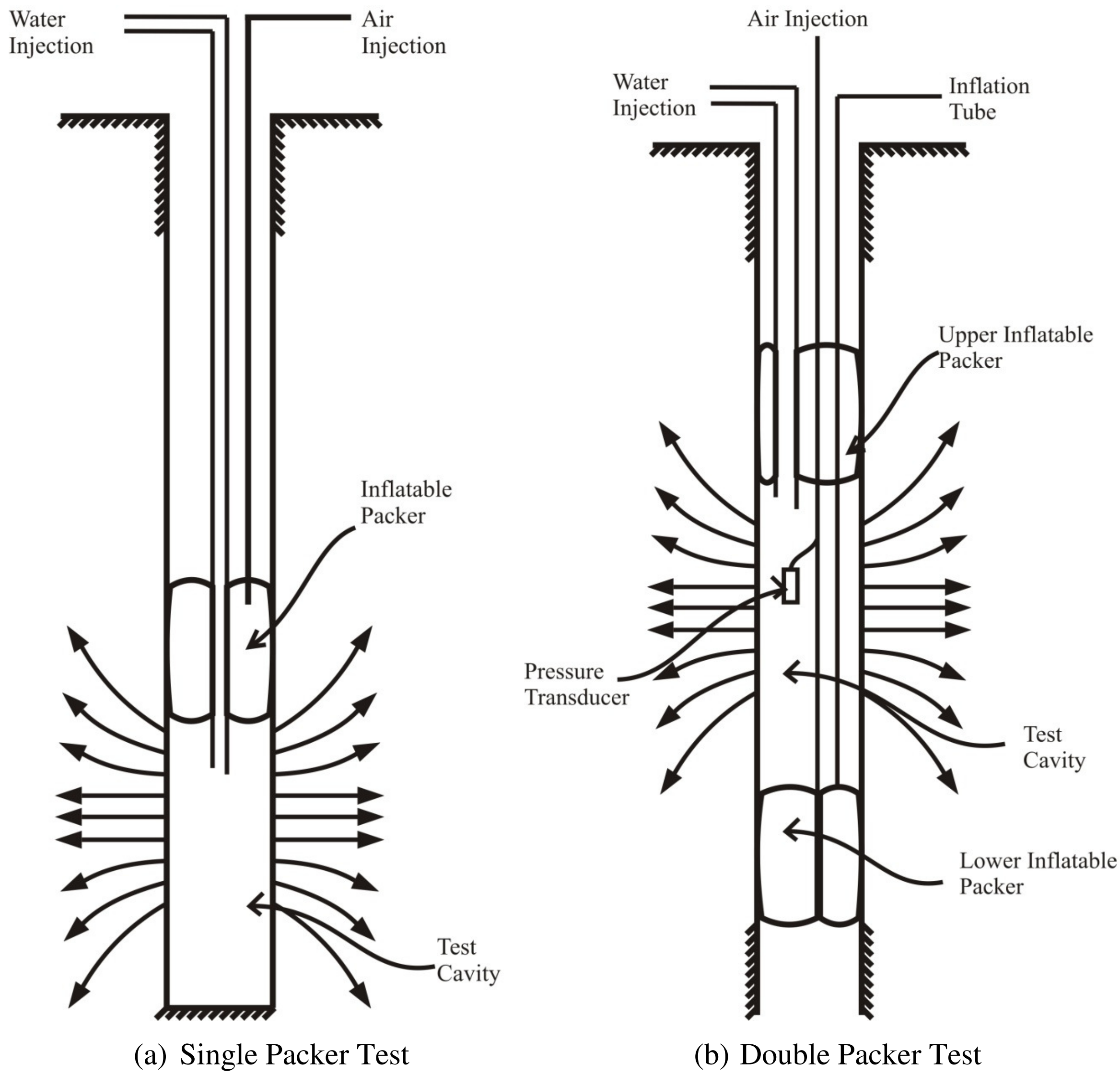

Figure 2.5 - Single and Double Packer Tests

2.3 - Documented Permeability Values of Indiana Limestone

Experimental results for the permeability of Indiana Limestone are documented in the articles cited in Table 2.1.

Table 2.1 - Reported Permeability Coefficients of Indiana Limestone

Reference	External Stresses	Permeation Direction	Permeating Fluid	Range of K ($10^{-15}m^2$)
(Heystee and Roegiers, 1981)	None	Radial	Nuto A10 Oil	1.3 to 1.4
(Suri et al., 1997)	None	Axial	Oil	6
(Bencsik and Ramanathan, 2001)	None	Not Mentioned	Not Mentioned	1.16+/-0.02
(Zeng and Grigg, 2006)	Hydrostatic Pressure (400psi)	Axial	Nitrogen Gas	21.6
(Selvadurai and Glowacki, 2008)	Confining Pressure (5MPa)	Axial	De-Aired Water	5.7 to 8
(Selvadurai and Selvadurai, 2009)	None	2-D	De-Aired Water	29.4 to 44.3

2.4 - Permeability of Rock Discontinuities

Rocks often contain natural fractures, which can affect the permeability and fluid transport characteristics. The increasing need to use and manage rock barriers to contain large quantities of contaminated material, such as crude oil, radioactive waste or even carbon dioxide, requires a better understanding of the hydro-mechanical properties of rock fractures and joints. Conventionally, the permeability of fractures is determined by in-situ tests and considered to be a constant property; in reality, however, most engineering activities such as underground excavations and groundwater lowering applications involve alterations in the geostatic stress field that changes the configuration of fractures (closing or opening) and eventually affects the permeability of these openings. Laboratory tests involving the permeability of fractures can be divided to two categories: The first deals with the study of natural rock joints that already exist in the core before being tested. Studies involving actual tests on natural joints are relatively scarce due to the difficulty of preserving the pre-excavation environment of the joint. On the other hand, several numerical models were developed to deal with natural joints. The second category involves fractures created in the laboratory (or artificial fractures). This section summarizes some literature involving these two categories.

Snow (1965) presented one of the early investigations that examined the influence of the externally applied normal and shear stresses on the alterations in the hydraulic conductivity of a fracture. Barton and Choubey (1977) present an empirical relation for determining the shear strength of rock joints. The authors relate the depth of weathering in rocks to permeability; high permeability rocks tend to be weakened throughout due to weathering while low permeability rocks develop weakened joint walls. Bandis et al. (1983) linked the importance of understanding the deformational response of rock joints with different roughness’s, wall strengths and aperture sizes to determine the permeability of jointed rocks. Other investigations of the hydraulic behaviour of joints and rock discontinuities were presented by Engelder and Scholz (1981), Walsh (1981), Gale (1982), Haimson and Doe (1983), Raven and Gale (1985), Bandis et al.(1986), Makurat et al. (1990), Boulon et al. (1993), Pyrak-Nolte and Morris (2000) and Selvadurai and Yu (2005).

Kranz et al. (1979) tested whole and jointed Barre Granite for permeability. The whole samples were 35mm in diameter and 90mm in length. Two types of jointed samples of the same dimensions were prepared: In the first type, specimens were created by clamping two smaller cylinders with parallel saw-cut faces to each other; the level of roughness of the joints was controlled to estimate its effects on the permeability. The second type of joint was created more "naturally" by initiating a tensile split along the length of the cylinder similar to Brazilian strength tests. The roughness of the tensile split joint is considered the highest (compared to the first type of joint). A triaxial cell was used for permeability measurements with Kerosene as the pressurizing and permeating fluid. Kerosene was chosen because it is non-reactive to the rock and thus chemical effects could be neglected. Transient pulse decay techniques were used to measure the permeability of the different samples. Cyclic pressure differentials were applied to the tension split cylinders while performing permeability tests. A hysteresis effect was showed permanent changes in the permeability after each cycle. It was also noticed that this phenomena decreased with increasing confining pressures. The effects of several variables such as effective stress, confining pressure, internal fluid pressure, temperature, and surface roughness on the permeability were also discussed in the paper.

Nguyen and Selvadurai (1998) developed a model to study the combined mechanical and hydraulic behavior of rock joints. Most previous models of rock joint behavior considered the joint surfaces as perfectly plane and only subjected to axial stresses, but this improved model takes into consideration "saw-tooth" joint surfaces and the presence of shear stresses that cause the dilation of the joint, which drastically affects its permeability. The model developed was implemented in a finite element code that was used to obtain numerical results for different experimental tests on joints, such as joints subjected to shear under normal stress, joints subjected to shear under constant stiffness, the effects of shear on joint permeability, and scale effects on joints. These numerical results were compared to experimental results with the same configuration and joint properties. The finite element model predicted acceptable results and performed satisfactorily.

Selvadurai (2008) tested the permeability of an artificial fracture induced in a large cylindrical Barre granite sample of 457mm in diameter and 510mm in height with a central axial cylindrical cavity of 57mm. The permeability of the sample in the intact state was first determined using the time dependant decay of hydraulic head at the pressurized cavity region, which creates radial flow through the sample. This type of test was chosen due to the obviously very low permeability of Barre Granite. A groove was machined around the sample at mid-height to force a fracture to occur at this specific location. Markers were installed on the surface of the sample to facilitate the re-assembly of the specimen after fracturing. Two diametrically placed steel wedges were used to apply a compressive load at the groove level resulting in the splitting of the cylinder. Complete separation of the sample was prevented during fracturing using a threaded rod inserted in the cavity connecting 2 rubber seats and 2 nuts at each side of the sample. The permeability of the fracture was determined at different levels of axial stress and LVDTs glued on the surface of the granite cylinder were used to determine the change in the fracture size. The permeability of the fracture decreased with the increase of the applied load as expected, but permanent changes in the permeability of the fracture were observed following several loading cycles.

Chapter 3 - Theoretical Background for Permeability

This chapter presents the fundamentals of the theory behind the measurement of permeability, mainly Darcy's Law and Laplace's Equation. The applications of those equations on specific configurations (rectilinear and radial flow) are discussed and the appropriate equations are derived. Finally, the parallel plate model for fluid flow in fractures is briefly discussed and the equations used for radial flow tests on fractured samples are presented.

3.1 - Darcy's Law and Laplace's Equation

The fundamental law describing fluid flow through porous media was proposed by Henri Darcy (1856) and was obtained by performing experiments on the flow of water through beds of sand. Darcy's Law is the basis of the concept of permeability in any porous material. The basic form of Darcy's Law is:

$$\nu = ki \tag{1}$$

where ν is the flow rate (m/sec), k is the hydraulic conductivity (m/sec) and i is the hydraulic gradient.

The main property under investigation in this research is permeability, which is often confused with hydraulic conductivity. The latter is actually dependant on both the material tested and the percolating fluid; on the other hand, permeability is an intrinsic property that is independent of the fluid. The hydraulic conductivity can be related to the permeability by the following equation:

$$k = \frac{\gamma_w}{\mu} K \tag{2}$$

where γ_w is the unit weight of water (N/m^3), μ is the dynamic viscosity of the fluid (N.sec/m^2) and K is the permeability of the porous medium (m^2).

The hydraulic gradient can be defined as the ratio of the difference in hydraulic heads at two points in a porous medium to the length over which that difference occurs. It takes the form:

$$i = \frac{h_1 - h_2}{L} = \frac{1}{\gamma_w L}(P_1 - P_2) \tag{3}$$

where h is the hydraulic head (m), L is the length over which the hydraulic head difference occurs (m) and P is the hydraulic pressure (N/m^2).

Darcy's Law can now be restated in the form:

$$Q = \frac{KA}{\mu L}(\Delta P) \tag{4}$$

where Q is the flow rate (m^3/sec), A is the cross sectional area through which the flow passes (m^2), ΔP is the differential pressure (N/m^2).

Darcy's Law can also be expressed in vector form:

$$\boldsymbol{v} = -k\nabla(h) \tag{5}$$

where ∇ is the vector differential operator (gradient).

“The Laplace equation is one of the most celebrated partial differential equations of Mathematical physics and has applications in the potential theory, electrostatics, elasticity, the theory of gravitation, magnetostatics, the theory of dielectrics, heat conduction and, most relevantly to this research, fluid flow in porous media” (Selvadurai, 2000). The flow of a fluid through a porous medium can be described by Laplace’s equation using Darcy’s Law and the mass conservation concept.

In fluid dynamics, the mass conservation equation (or continuity equation) states that in any steady state process, the rate at which mass (fluid) enters a system is equal to the rate at which mass leaves the system. Assuming the fluid is incompressible and the porous medium is non-deformable, the mass conservation equation applied to fluid flow is of the form:

$$\frac{\partial v_x}{\partial x} + \frac{\partial v_y}{\partial y} + \frac{\partial v_z}{\partial z} = 0 \tag{6}$$

in vector differential form:

$$\nabla.(\boldsymbol{v}) = 0 \tag{7}$$

Combining Darcy’s Law (5) with the mass conservation equation (7) and assuming k is constant throughout the porous medium results in Laplace’s basic equation (8) for the flow of a fluid through an isotropic porous medium.

$$\nabla.\{\nabla(h)\} = \nabla^2(h) = \left(\frac{\partial^2}{\partial x^2} + \frac{\partial^2}{\partial y^2} + \frac{\partial^2}{\partial z^2}\right)h = 0 \tag{8}$$

where ∇^2 is the Laplace operator.

3.2 - Permeability in Rectilinear Steady Flow Tests

The Laplace equation can define the rectilinear flow through a porous medium by applying a set of boundary conditions. Equations 9 and 10 represent, respectively, the one-dimensional equivalent of the Laplace equation for fluid flow in a porous medium (8) and its corresponding most general solution (Selvadurai, 2000):

$$\frac{d^2h}{dx^2} = 0 \tag{9}$$

$$h(x) = A_1x + A_2 \tag{10}$$

where A_1 and A_2 are arbitrary constants.

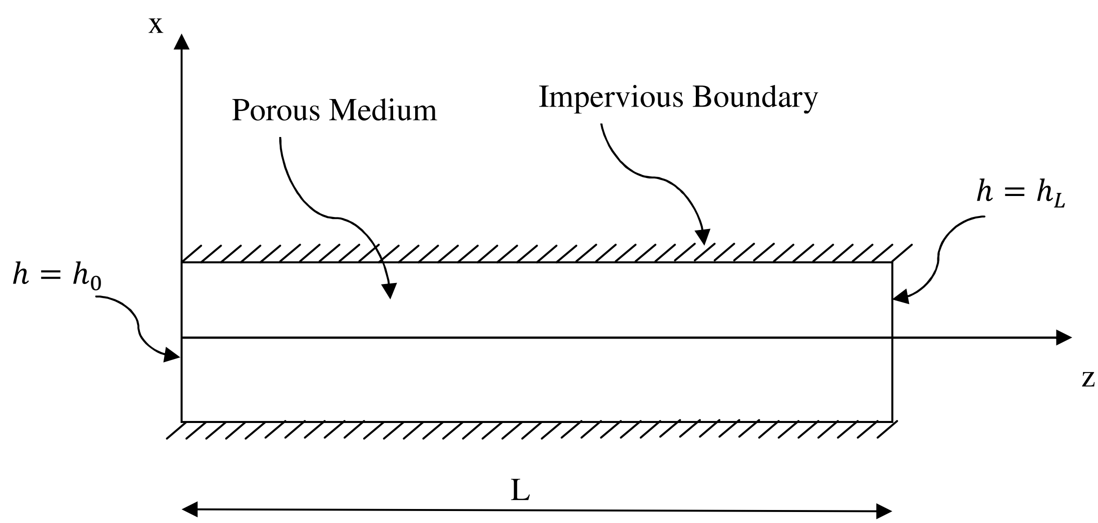

Figure 3.1 - One-Dimensional Flow in a Porous Element

Applying the boundary conditions shown in Figure 3.1, Equation 10 takes the form:

$$h(z) = h_0 - \frac{z}{L}(h_0 - h_L) \tag{11}$$

Considering Darcy's Law:

$$v_z(z) = -k\frac{dh}{dz} = k\frac{(h_0 - h_L)}{L} \tag{12}$$

or:

$$K = \frac{\mu}{\gamma_w}k = \frac{Q\mu L}{A\gamma_w(h_0 - h_L)} \tag{13}$$

Equation 13 represents the equation of permeability in a one-dimensional steady flow test.

3.3 - Permeability in Steady Radial Flow Tests

The Laplace equation can define the one-dimensional radial flow through a porous medium by first expressing the equation in axisymmetric plane polar coordinates and second applying the correct boundary conditions. Equations 14 and 15 represent, respectively, the one-dimensional equivalent of the Laplace equation for radial fluid flow in a porous medium and its corresponding solution (Selvadurai, 2000):

$$\frac{d^2h}{dr^2} + \frac{1}{r}\frac{dh}{dr} = 0 \tag{14}$$

$$h(r) = B_1 \log_e r + B_2 \tag{15}$$

where B_1 and B_2 are arbitrary constants.

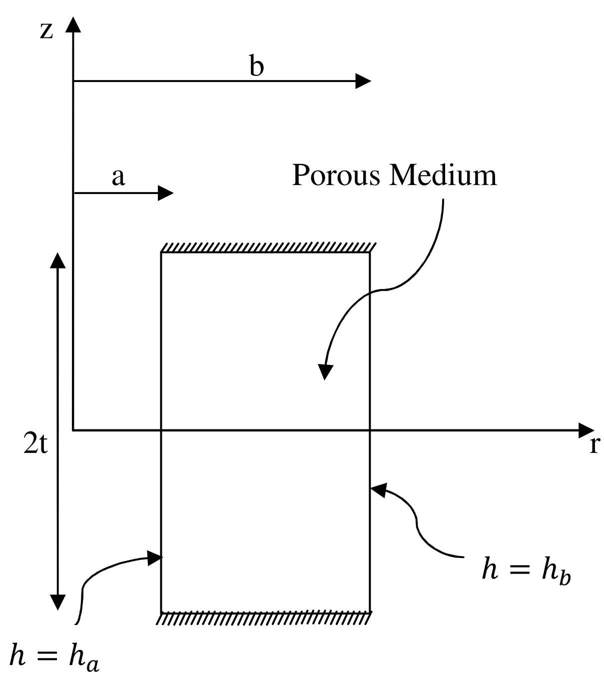

Figure 3.2 - One-Dimensional Radial Flow in a Porous Layer

Applying the boundary conditions shown in Figure 3.2, Equation 15 takes the form:

$$h(r) = h_a - (h_a - h_b)\left(\frac{\log_e(r/a)}{\log_e(b/a)}\right) \tag{16}$$

Considering Darcy's Law:

$$v_r(r) = -k\frac{dh}{dr} = k\frac{(h_a - h_b)}{r\log_e(b/a)} \tag{17}$$

or:

$$K = \frac{\mu}{\gamma_w}k = \frac{Q\mu\log_e(b/a)}{2\pi t\gamma_w(h_0 - h_L)} \tag{18}$$

where K is the permeability of the porous medium (m^2), Q is the flow rate (m^3/sec), μ is the dynamic viscosity of the fluid (N.sec/m^2), γ_w is the unit weight of water (N/m^3), b is the radius of the sample (m), a is the radius of the cavity (m), $2t$ is the length of the sample (m) and $h_0 - h_L$ is the hydraulic head difference across the sample's radial direction (m).

Equation 18 represents the equation of permeability in a one-dimensional radial steady flow test.

3.4 - Permeability of Fractures in Rocks

The main objective of the research is the examination of the reduction in permeability of the fracture with quasi-cycled loading normal to the fracture plane. Two general laboratory configurations, radial flow and linear flow, are commonly used to determine the permeability of the fracture. In radial flow fracture permeability tests (Iwai, 1976; Raven and Gale, 1985), a fracture, perpendicular to the axis of the cylindrical sample is introduced and subjected to normal stress, constant fluid flow is applied to a concentric axial cylindrical cavity that intersects the fracture plane, and the permeability is determined by measuring the drop in head between the cavity and the outer surface of the sample. In the linear flow method (Kranz et al., 1979; Trimmer et al., 1980) the axis of the sample is contained in the fracture plane and the normal stress is applied by confining the sample in a triaxial cell.

The cubic law, also known as the parallel plate model represents the fracture as two parallel plates separated by a constant distance (aperture). Equation 19 presents the cubic law for one-dimensional water flow (National Research Council, 1996):

$$Q = \frac{t^3}{12\mu} \nabla P \tag{19}$$

where t is the aperture size (m) and ∇P is the pressure gradient (N/ m^2).

Selvadurai (2008) presents the formulas (20, 21) used for radial flow fracture permeability tests that are based on the parallel plate model.

$$K_f = \frac{\mu Q_f}{4\pi t(p_i - p_e)} \log_e \left(\frac{b}{a}\right) \tag{20}$$

where b is external radius of the sample (m), a is radius of the cavity (m), p_i is the cavity pressure at steady state (N/m^2), p_e is the pressure on the cylindrical exterior surface at steady state (N/ m^2), Q_f is the flow rate in the fracture (m^3/sec), K_f is the permeability of the fracture (m^2).

While the majority of the flow occurs in the fracture, some flow is expected to occur in the rock matrix, especially when the fracture aperture size decreases at high loads. Thus, the permeability of the intact rock (K_i) influences the permeability of the fractured sample as stated in the following equation:

$$K_f = \left(\frac{\mu Q}{4\pi\sqrt{3}(p_i - p_e)} \log_e \left(\frac{b}{a} \right) - \frac{K_i l}{2\sqrt{3}} \right)^{2/3} \tag{21}$$

where K_f is the permeability of the fracture (m^2), K_i is the permeability of the intact rock (m^2), Q is the total flow rate (m^3/sec), μ is the dynamic viscosity of the fluid (N.sec/m^2), b is the radius of the sample (m), a is the radius of the cavity (m), p_i is the cavity pressure at steady state (N/m^2), p_e is the pressure on the cylindrical exterior surface at steady state (N/ m^2), and l is the length of the sample (m).

Chapter 4 - Indiana Limestone

This chapter presents an overview of Indiana Limestone, the material tested in this research. A brief history of the use of the stone since the earliest excavations, its geological formation, its different categories and types and its mechanical and physical properties are discussed. Finally, the procedures followed to prepare the samples for the experiments are detailed.

4.1 - Brief History

The 18th Edition of the Indiana Limestone Institute of America Inc. Handbook (1998) traces the earliest excavations and uses of Indiana Limestone to the early 1800s. This stone was discovered in Indiana, USA, and was used for simple cabin foundations. The light color of Indiana Limestone attracted architects and its relative easy machinability attracted structural projects such as railroads and large terminal facilities. Indiana Limestone was also preferred for its high resistance to fire which was noticed during the 1871 and 1872 fires of Chicago and Boston respectively. Indiana Limestone is still widely used by builders and architects, especially following the advancement of quarrying and machining techniques.

4.2 - Geological Formation

The formation of Indiana Limestone, also known as Salem Limestone, dates back 300 million years to the Mississippian geological era. It is mainly formed of calcite ($CaCO_3$), a cementing material that binds skeletons of marine origin. Crushed sea shells as well as small quantities of iron bearing minerals, clay and organic materials are found throughout Indiana Limestone formations (ILIA, 1998).

4.3 - Classification

The main characteristics that differentiate different types of Indiana Limestone as classified by the Indiana Limestone Institute are grade and color. Buff and grey are the two main colors, while Select, Standard and Rustic are the main grade categories, which, in that order, indicate the presence of, from least to most, calcite streaks or spots, fossils or shelly formation, pit holes, reedy formations, open texture streaks, honeycomb formations, iron spots, travertine-like formations and grain formation changes. A very special category is the Variegated Indiana Limestone; this consists of a combination of all the colors and grades and is thus considered to be the least homogenous type of this rock formation (ILIA, 1998).

4.4 - Physical Properties

The following table summarizes some physical and mechanical properties of Indiana Limestone reported by the 18th edition of the Indiana Limestone Institute of America Inc. (ILIA, 1998).

Table 4.1 - Mechanical and Physical Properties of Indiana Limestone (ILIA, 1998)

Property	**Value**
Ultimate compressive strength of dry specimens	28MPa (4000psi)
Modulus of rupture of dry specimens	4.8MPa (700psi)
Absorption	7.5%
Bulk specific gravity	2.1 to 2.75
Modulus of elasticity	2.3 to 37.2GPa (330 to 5400ksi)
Ultimate shear strength	6.3 to 12.4MPa (900 to 1800psi)
Ultimate tensile strength	2.1 to 4.9MPa (300 to 715psi)
Density	2306kg/m^3 (144lbs/ft^3)

4.5 - Sample Preparation

Six cylindrical cores of 150mm diameter and 300mm length were retrieved from one Indiana Limestone block of dimensions approximately 400mm×400mm×300mm dimensions that was stored at 6.6 °C. The cores were numbered to keep a reference of their original location within the block (Figure 4.1). The block was one of several supplied by Primcar Inc. Les Pierres, from Montreal. The specimens tested by Selvadurai and Glowacki (2008) were retrieved from another block provided by the same supplier. Selvadurai and Glowacki (2008) performed tests on the Indiana Limestone to determine the mechanical and physical properties, which are summarized in the following table:

Table 4.2 - Mechanical and Physical Properties of Indiana Limestone (Glowacki, 2008)

Property	Value
Modulus of elasticity	24GPa
Ultimate compressive strength	37.5MPa
Ultimate tensile strength	3.6MPa
Density	2243Kg/m^3
Poisson's ratio	0.14
Porosity	16.60%

Figure 4.1 - Original Block with Referenced Cores

The cylindrical surfaces of the cores were first machined to a smooth finish on a lathe using a carbide-tipped boring bit to obtain cylinders 100mm in diameter. A Vee-groove was introduced at the mid-plane of the sample to facilitate the introduction of a flat fracture normal to the axis of the cylinder (Figure 4.2). The groove was further deepened with an extra sharp tool bit to minimize the possibility of having a fracture propagating outside the groove. The final groove dimensions were of 2mm width, 1.8mm depth and a groove angle of 60°.

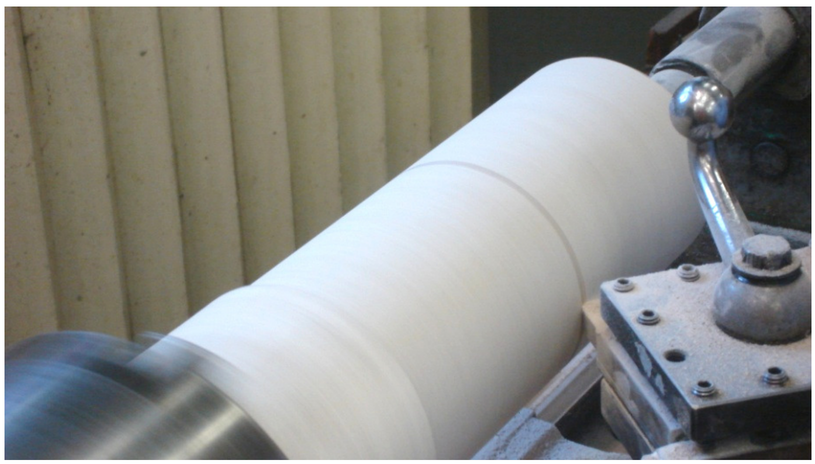

Figure 4.2 - Introducing a Vee-Groove on the Sample

A cylindrical central cavity of diameter 20mm was drilled in the sample using an SDS-Shank Rotary-Hammer drill bit supplied by McMaster-Carr. Since the flow is initiated from the central cavity, it is essential that the cavity surface be free of debris that might have accumulated during the drilling process. To avoid any undue influence of the debris clogging of the surface pores of the central cavity, the drilled cavity is further bored to a final diameter of 23mm using a Carbide-tipped Boring tool supplied by McMaster Carr.

Figure 4.3 a and b show respectively the drilling and boring processes, where the sample was covered using the non adhesive side of black duct-tape to avoid damaging the surface of the sample where it is clamped to the lathe.

(a) Drilling the Sample

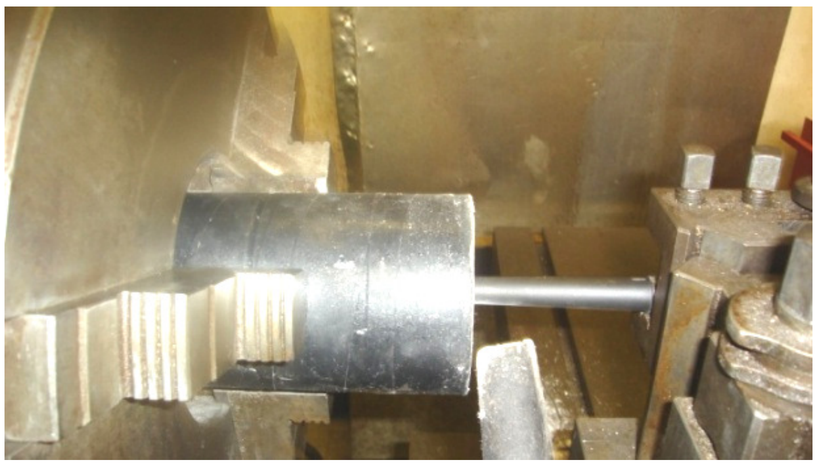

(b) Boring the Sample's Cylindrical Cavity

Figure 4.3 - Machining the Sample

The samples were cut to obtain cylinders of 200mm lengths with plane ends ground to a smooth finish. An epoxy coat of 1mm thickness was applied to the upper and lower plane faces of the samples. The epoxy used consisted of a mix of Bondo Marine epoxy resin and liquid hardener. The extra epoxy around the edge of the flat surfaces was removed by grinding and the excess epoxy covering the central cavity was drilled to provide access to the internal cavity. The cavity was inspected for any debris, which was removed to prepare the sample for testing (Figure 4.4).

Figure 4.4 - Sample Ready for Testing

Equally spaced above and below the groove, 2 Demec points were glued to the sample, using the same Bondo Marine epoxy resin, at 3 locations around the sample to measure the initial fracture aperture size after fracturing the samples. The central cavity of the samples was then subjected to approximately 12 hours of vacuum pumping at a pressure of approximately 80kPa. The resulting converging radial flow helped to flush out any debris remaining on the cavity surface and to saturate the sample. Figure 4.5 shows the final appearance of the samples prior to vacuum saturation and Figure 4.6 shows schematic diagrams of the samples, summarizing all the dimensions.

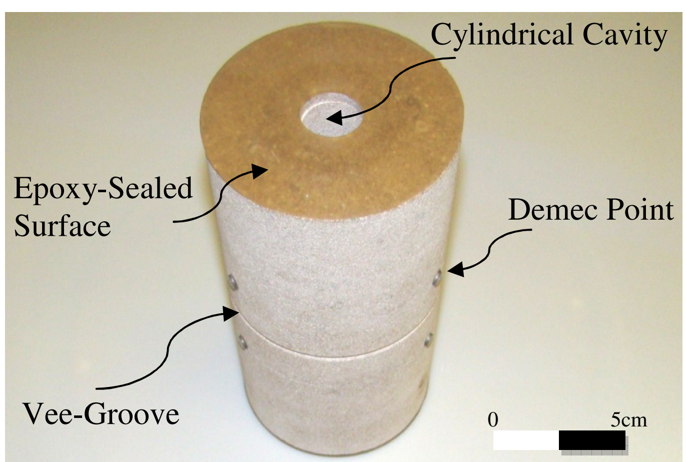

Figure 4.5 - Final Appearance of the Sample Showing the Demec Points

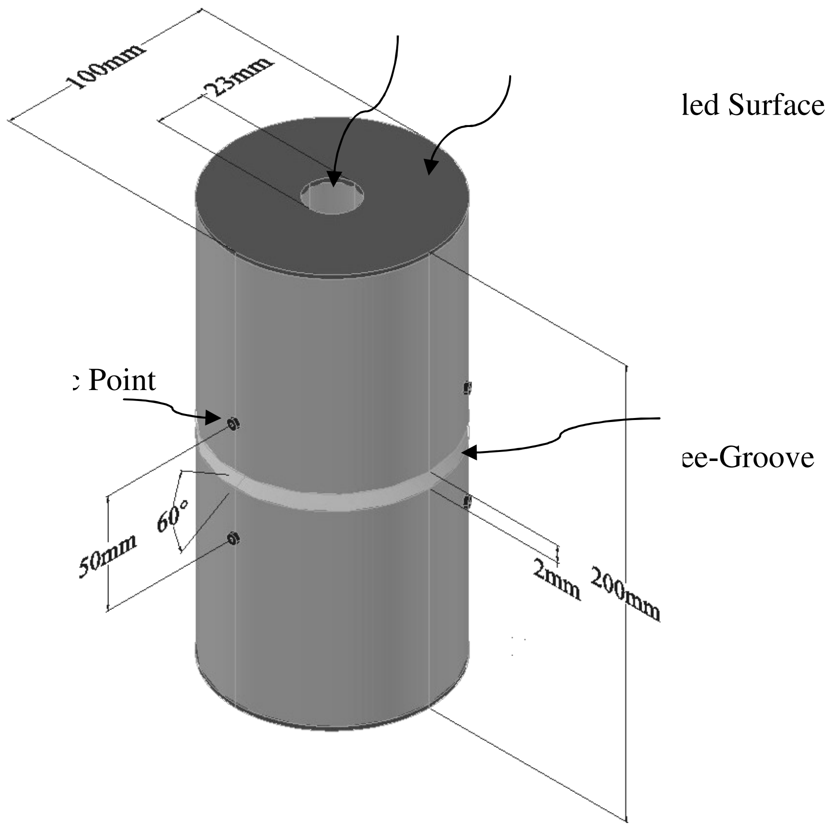

(a) Schematic View of the sample

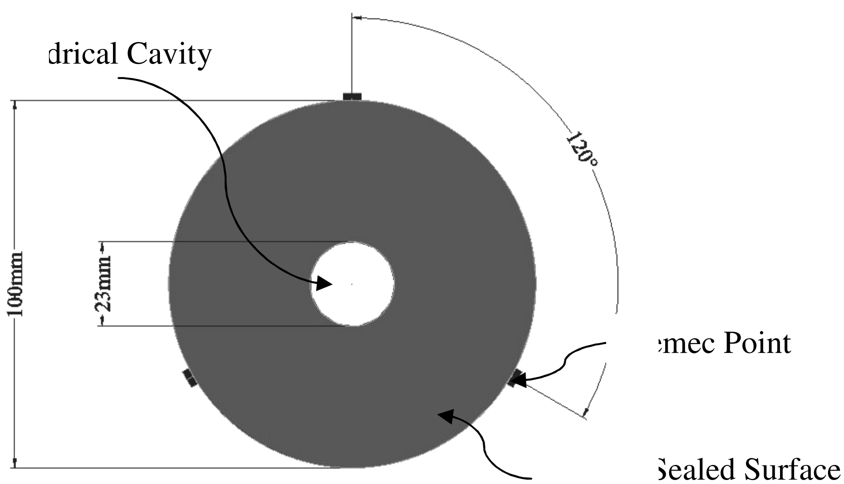

(b) Schematic Top View of the Sample

Figure 4.6 - Schematic View of the Indiana Limestone Sample

Chapter 5 - Experimental Procedure and Components

This chapter presents the procedures followed to measure the permeability of intact, fractured and sealed Indiana Limestone samples. The assembly of the components of the experimental facility and the method used to fracture the samples are fully discussed.

5.1 - Permeability Testing of Intact Samples

The steady state constant flow method was used to test the permeability of the six Indiana Limestone samples. Radial water flow was applied through the cylindrical cavity to reach a steady internal water pressure. This section describes the experimental procedures that were used to determine the steady state pressure as well as the main components of the experimental facility. Figure 5.1 presents a schematic view of the test facility.

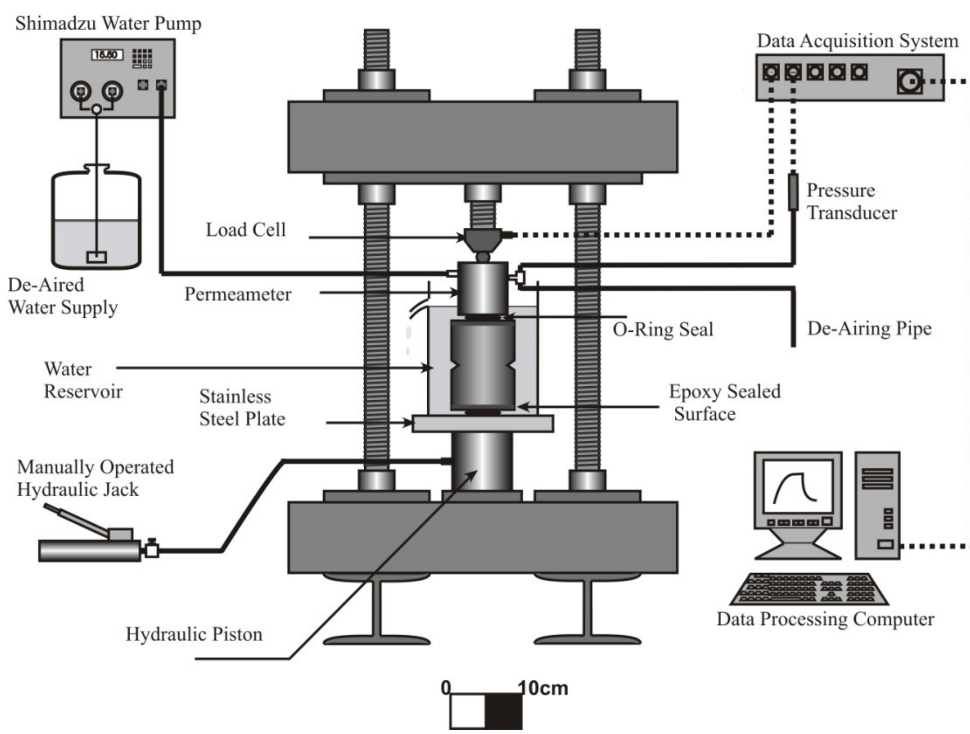

Figure 5.1 - Schematic Diagram Summarizing Experimental Facility for Permeability Testing of Intact Specimens

A cross-sectional view of the sample (Figure 5.2) shows two of the main components of the setup, the permeameter and the sealing system.

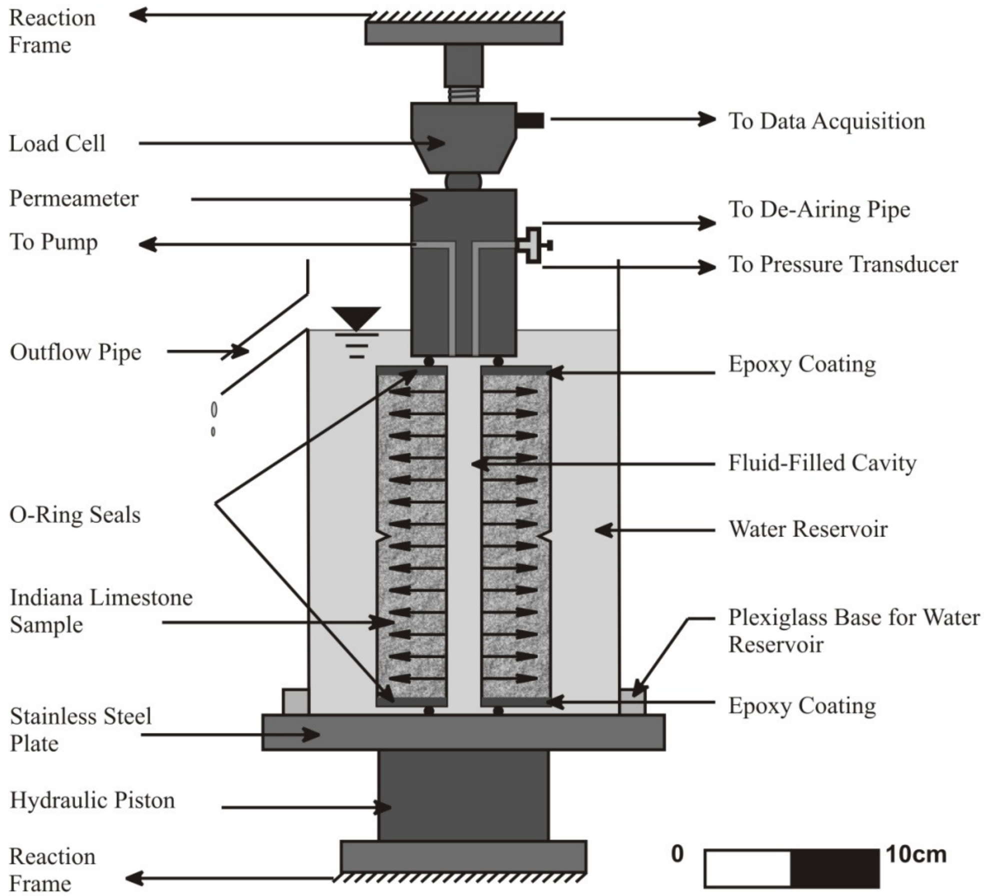

Figure 5.2 - Cross-Sectional View of the Sample and the Permeameter

The main functions of the permeameter include the de-airing of the water-filled cavity and conveying water to the sample. The permeameter is made of a non-corrosive stainless steel. The cross section of the permeameter (Figure 5.2) shows the mechanism in which water conveyed from the pump (a Shimadzu LC-8A liquid transfer unit with a flow rate range of (0.1 to 150)mL/min) fills the cylindrical cavity through the first permeameter opening. The cavity de-airing and filling is considered complete when the outflow shows a steady water flow with no visible air. The second permeameter opening is connected to a two way valve originally conveying the flow to a de-airing pipe; once the system is completely de-aired, the two way valve can be switched to the 1.4MPa (200psi) range Honeywell pressure transducer (Model TJE) of 0.1%accuracy (supplied by Hoskin Scientific).

A closed system between the pump, the pressure transducer and the internal cavity of the sample is essential for the success of the experiments; this necessitates an effective sealing system. The Buna Neoprene 70 Durometer O-rings, coated with Dow Corning high vacuum grease, were used to provide the seal. The O-rings have 40mm internal diameters, 50mm external diameters and a cross-sectional thickness of 4mm. The permeameter and the stainless steel plate on which the sample is positioned had circular grooves that served as seats for the O-rings, which prevented any radial expansion during either the application of the axial load or the increase of the cavity pressure. The axial load was applied using an Enerpac hydraulic piston controlled by a 6.9Mpa (10000psi) Enerpac hydraulic jack; the steel reaction frame that was used in the experimental facility transferred the load to the sample. A sealing pressure of 2MPa was enough to prevent any leakage and was used in all the experiments on the intact samples. The load was constantly measured using an Interface load cell (Model 1200 Precision Series) with a maximum capacity of 45kN.

The water reservoir was made of a 200mm diameter plexiglas tube glued to a stainless steel plate. The reservoir kept and maintained a constant external pressure head through an overflow pipe connection.

The data acquisition-system consisted of 2 Dataforth Signal Conditioning Modules (Model SCM5B, supplied by A-Tech Instruments) that filter, isolate, amplify, and convert the input signal from the pressure transducer and the load cell to a high-level analog voltage. The output voltage is read, converted and graphically displayed by TracerDAQ Pro software installed on a PC. The water temperature was manually recorded at the beginning and end of each test using a digital thermometer connected to the water input reservoir. Figure 5.3 shows the experimental facility with all the components used for testing the permeability of the intact cylinders of Indiana limestone.

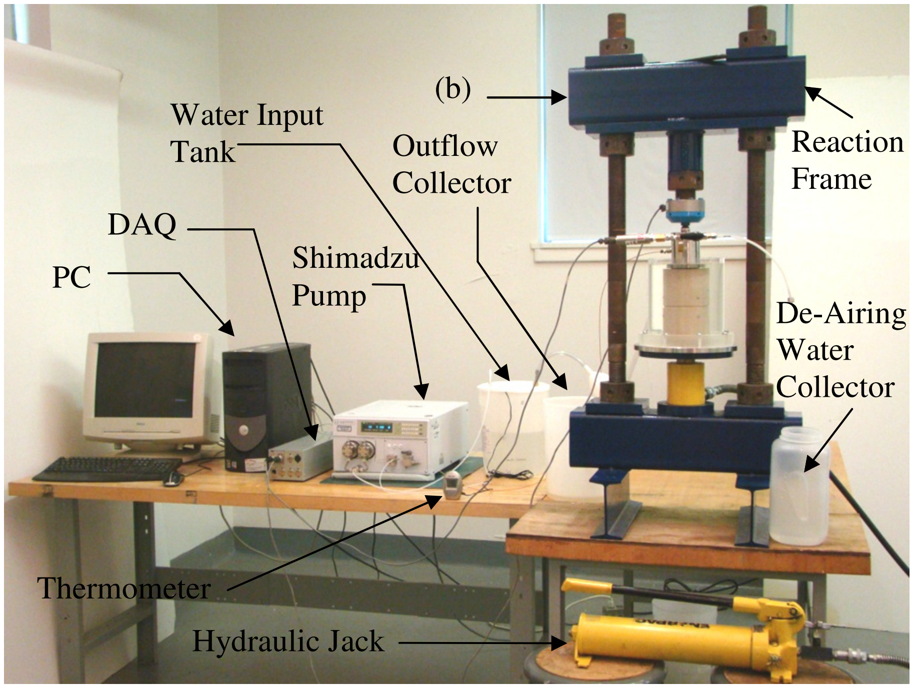

(a) The Test Facility and Components

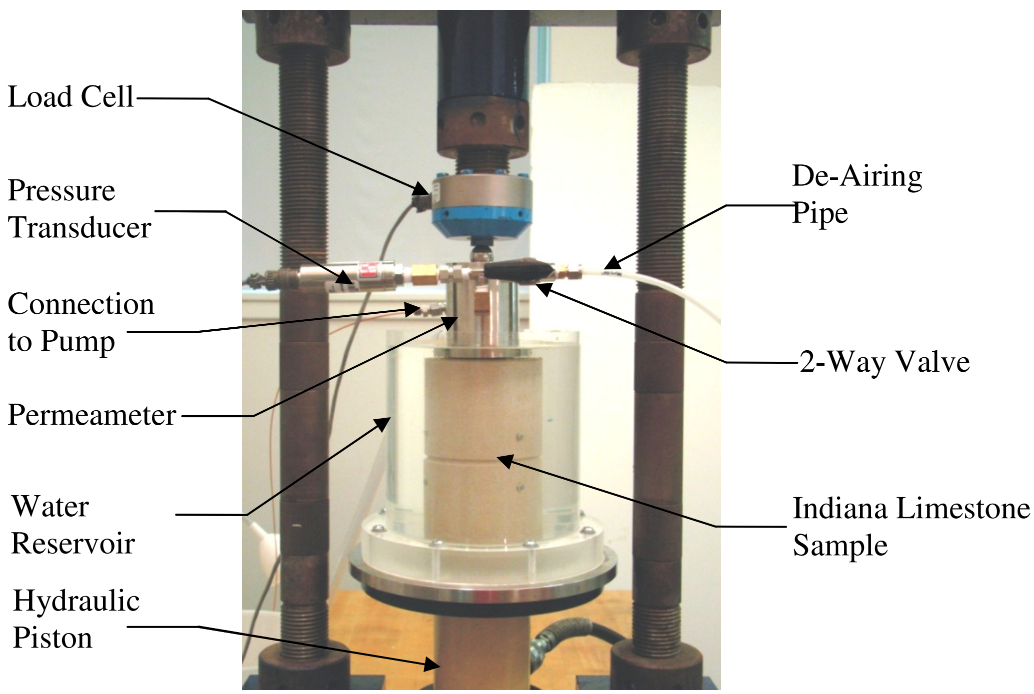

(b) Close View on the Sample in The loading Frame

Figure 5.3 - The Test Facility and Components

A brief summary of the procedure used to determine of the permeability of the intact cylinders is as follows:

- The saturated sample is centered on the lower O-ring located on the stainless steel plate. The upper O-ring and the permeameter are positioned centrally on the sample.
- A load equal to or higher than the load required to seal the system is applied and the load cell and pressure transducer are connected to the data acquisition system.
- A flow of 2, 3 or 5mL/min is applied. When de-airing is complete, the 2-way valve is switched from the de-airing pipe to the pressure transducer.
- The evolution of pressure is recorded until a steady pressure and the temperature monitored throughout the test.
- The procedure is repeated at least 5 times with different flow rates to obtain repeatable results.

5.2 - Fracturing the Samples

This section presents the procedure followed and components used to create a flat fracture positioned at the groove. Two "dummy" samples of Indiana Limestone used in previous research were first used to finalize all aspects of the fracturing procedure without the risk of damaging any of the six samples. Consequently, several important factors were identified to control the fracturing procedure. First, the groove created on the sample should be as sharp as possible to minimize the development of a fracture beyond the position of the groove. Second, it was important to measure the initial fracture aperture size; this lead to the installation of the Demec points as discussed in Chapter 4. Figure 5.4 shows the use of a dial gage with a precision of 0.0125mm to measure the distance between the Demec points prior to fracturing the samples.

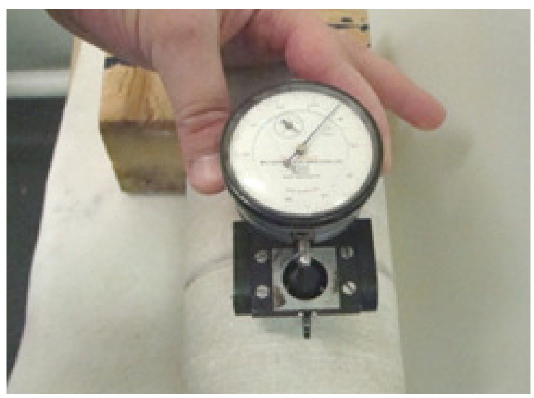

Figure 5.4 - Measuring the Initial Fracture Aperture Size

Another essential factor identified was to make sure that the two halves of the fractured sample were held together at all times in order not to lose any debris and to maintain the initial positioning between the two parts; an assembly consisting of a threaded rod of diameter 20mm and length 250mm inserted in the cavity of the sample and two hex-nuts assembled to the rod on both sides of the sample to apply a compressive load through the axial direction was implemented (Figure 5.5). Rubber seats and washers were placed between the nuts and the epoxy-coated surface of the sample to leave room for the fracture to occur and a torque of 10.8N-m was used to tighten the two hex-nuts.

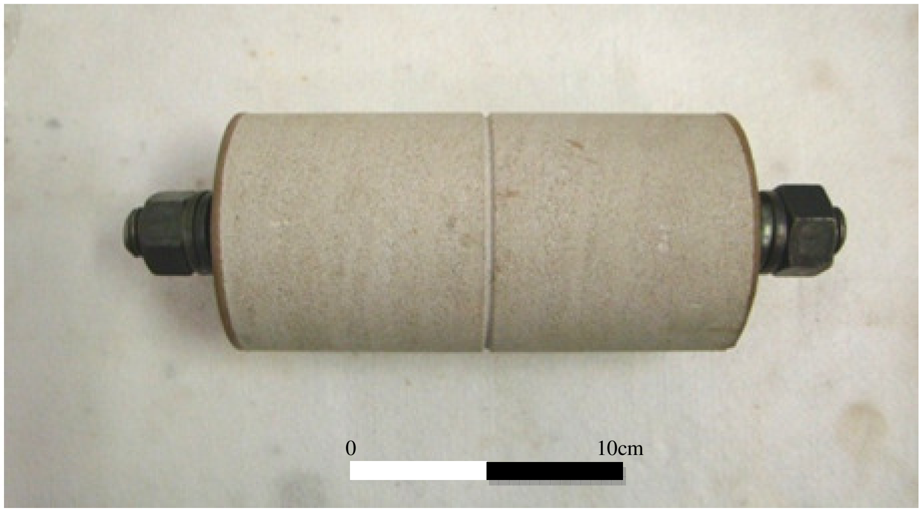

(a) Sample with Threaded Rod Assembly

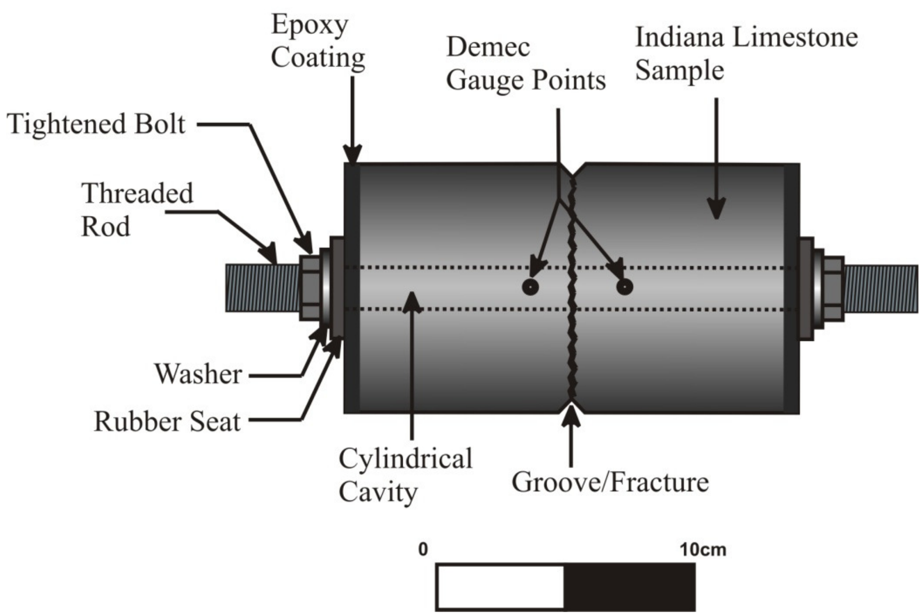

(b) Schematic View of the Threaded Rod Assembly

Figure 5.5 - Threaded Rod Assembly

The fracture should be initiated without a preferential direction in a tensile rather than a bending mode. Bending of the sample can create different types of fractures over the fracture. A double diametral compression test for the tensile strength testing of rock was thus performed using an MTS rock splitting machine located on the Structures Laboratory of the department of Civil Engineering and Applied Mechanics. This procedure resulted in the creation of a clean flat fracture and the reduction of damage at the contact points (due to four loading points instead of the conventional two). In addition, the results of the splitting test can be used to determine the tensile strength of Indiana Limestone which varied from 3.2 to 3.8MPa. The jig for fracturing the samples (Figure 5.6) was machined using 37.5mm thick cold rolled steel plates and consisted of two V-Blocks each connected to a square plate. Two circular slots were machined in the "V" to hold 5mm diameter rods that would serve as "splitters" when in contact with the sample's groove. The two splitters are identical with the exception of 2 bolts on the lower splitter that are used to hold the sample in place after the fracture propagates and the load is released. Figure 5.7 shows the sample and the splitting fixture in the MTS Rock Testing Machine. The testing machine was then programmed to apply the load at 0.05kN/sec. The release time can be specified by entering the desired load drop as a percentage of the maximum load. The distance between the two Demec points at each of the three locations on the sample were then re-measured and recorded. The average of these values provided the initial aperture size of the fracture.

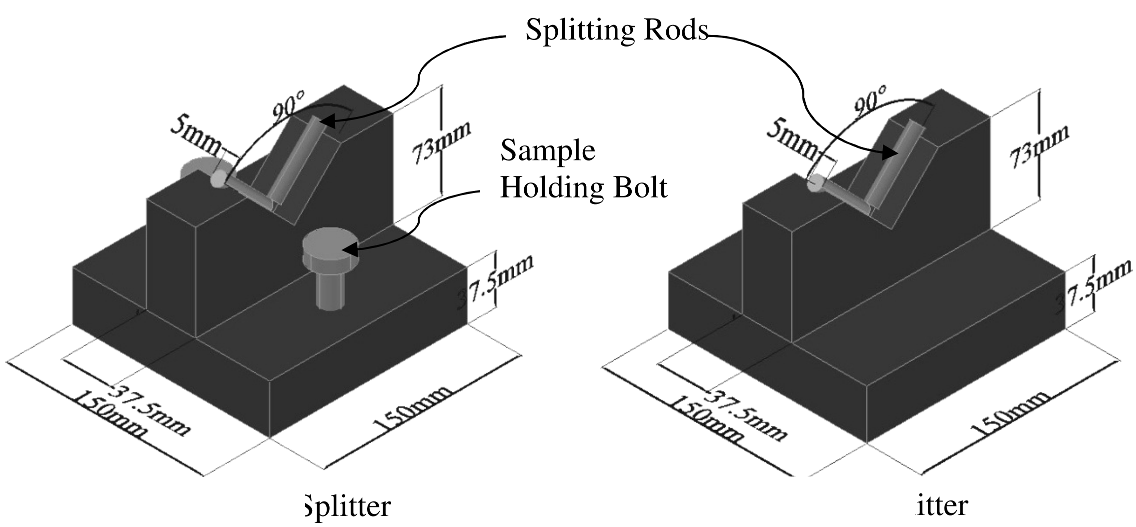

Figure 5.6 - Schematic View of Splitter Blocks

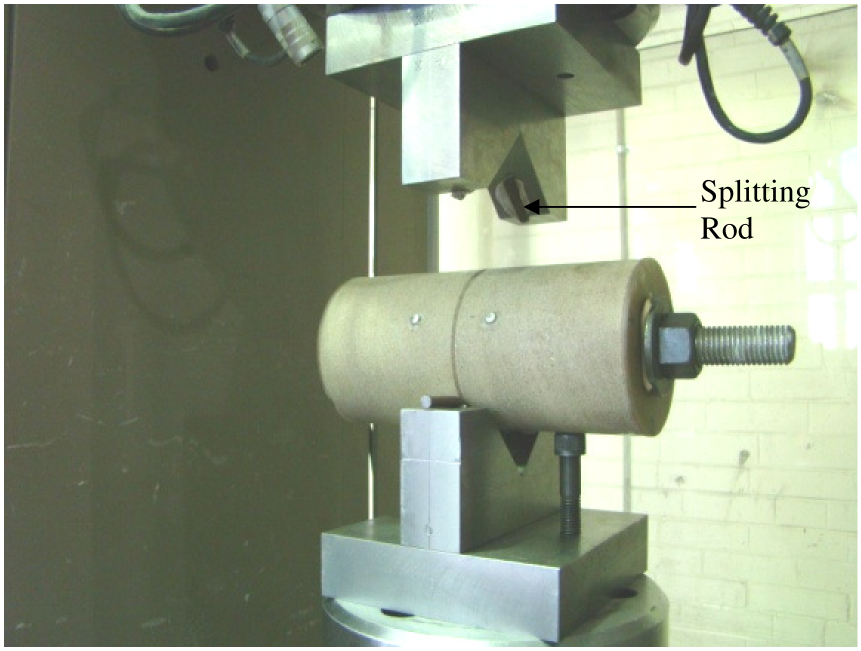

(a) Sample in Splitting Fixture

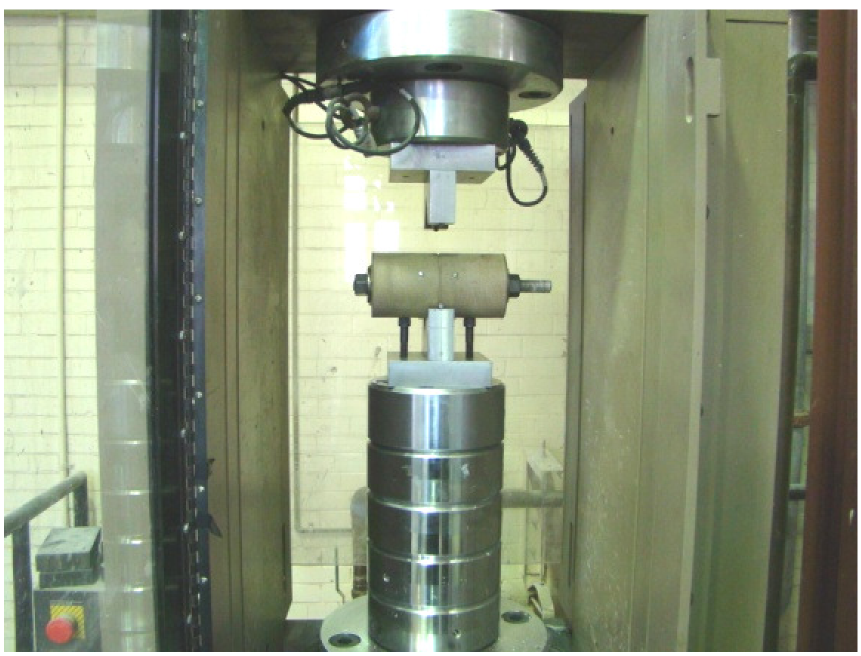

(b) Splitting Fixture in the MTS Rock Testing Machine

Figure 5.7 - Fracturing the Samples

5.3 - Permeability Testing of Fractured Samples

This phase of the research involved the determination of the permeability of the fracture under stress cycling. The central threaded rod system (Figure 5.5) was replaced by another system that fits in the water reservoir and can maintain two halves of the sample as a single unit. Digital indicators were installed in order to measure the fracture size evolution at three different locations (preferably the same as the Demec point locations). Figure 5.8 shows a schematic view of the experimental facility for testing the fractured samples.

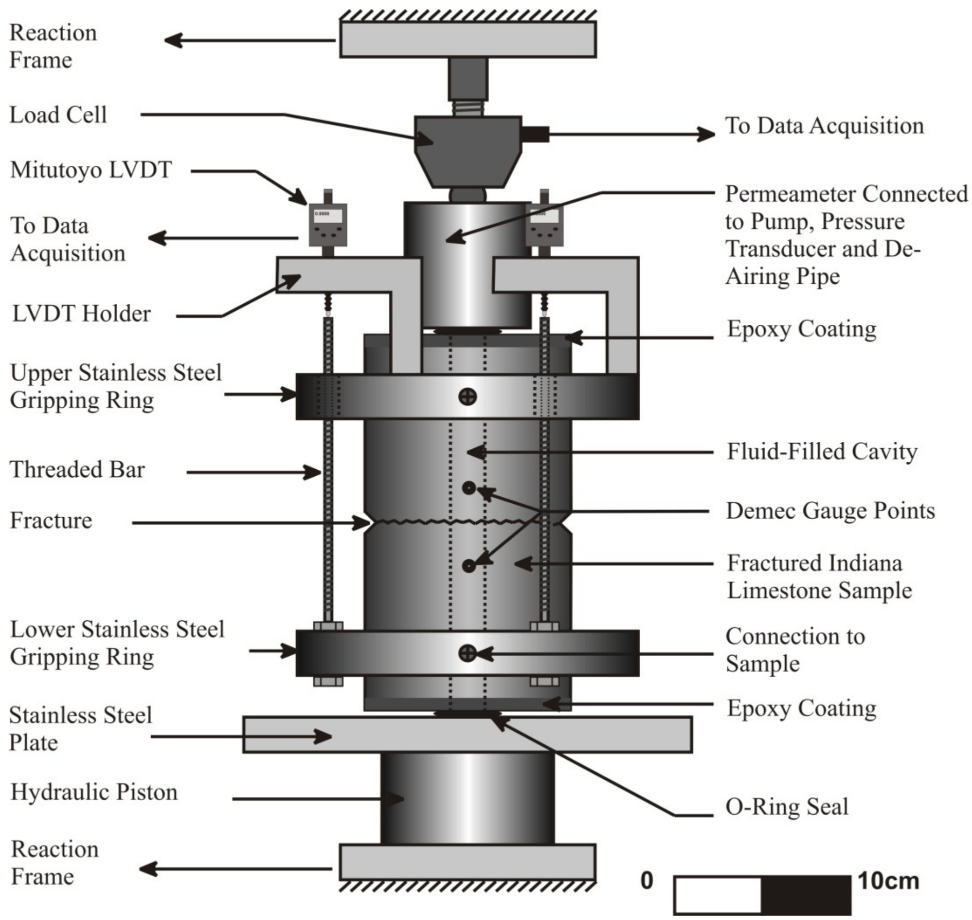

Figure 5.8 - Schematic View of the Sample Holder and LVDT Arrangements for Permeability Testing of Fractured Cylinders

The mechanism used to replace the central threaded rod system consisted of two gripping stainless steel rings (a lower ring and an upper ring), three threaded bars, and six sharp screws. The three bars are fixed to the bottom ring as shown in Figure 5.9. The three sharp screws are screwed halfway in three threaded holes on the sides of the bottom ring as well as on the sides of the upper ring. The upper ring holds three plexiglas fixtures (LVDT Holders) that serve as holders for the LVDTs that are used to measure the change of the aperture of the fracture (Figure 5.9).

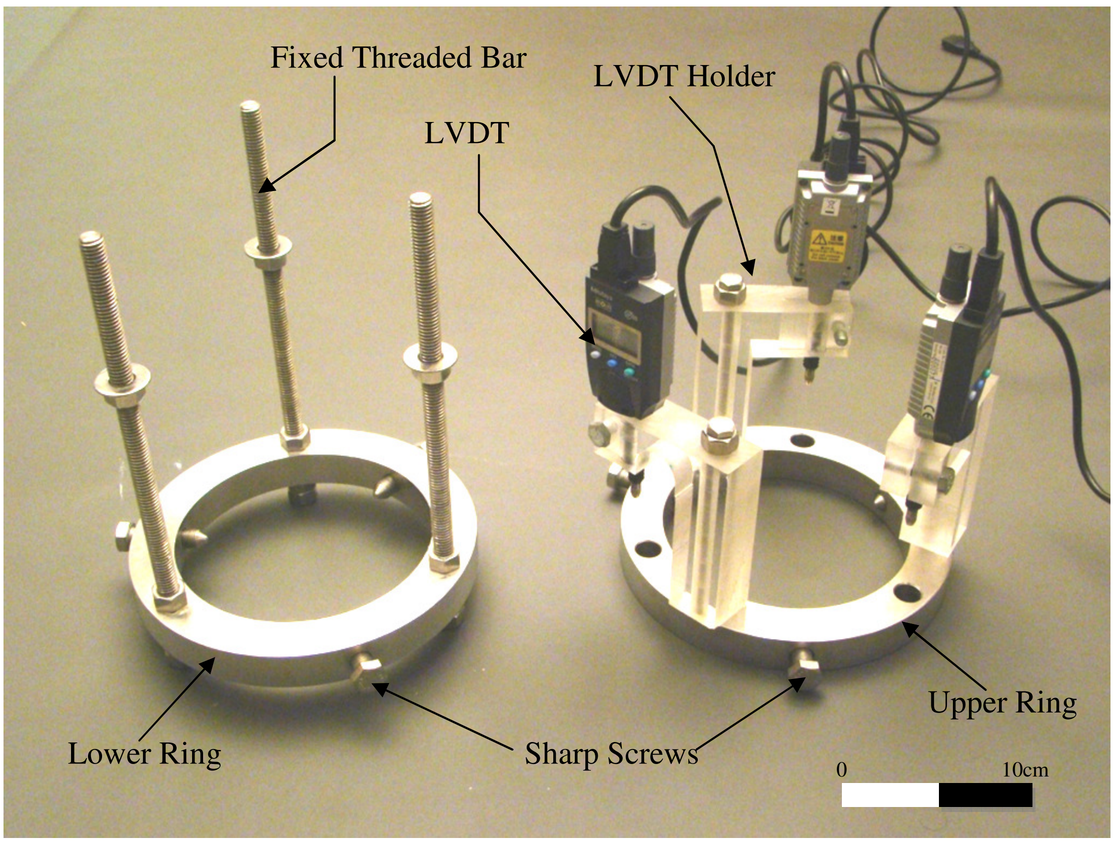

Figure 5.9 - Lower Ring with three Fixed Threaded Bars and Upper Ring with LVDT Holders

The sample with the central threaded rod system still in place is first centered within the lower ring (Figure 5.10-a), and the 3 sharp screws are tightened to provide a good grip between the lower ring and the lower part of the fractured sample (Figure 5.10-b). The upper stainless steel ring is connected to the upper part of the sample using 3 sharp screws similarly to the lower ring (Figure 5.10-c).

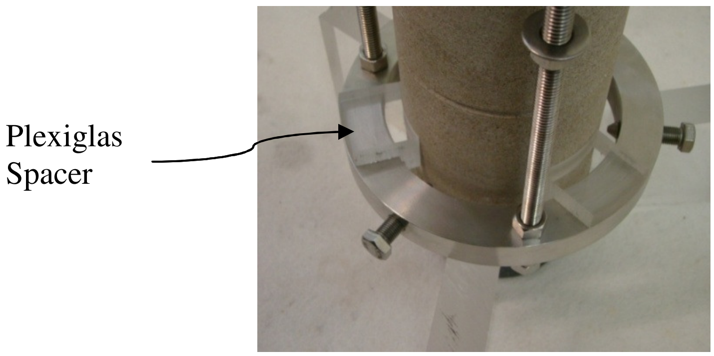

(a) Sample Centered in the Lower Gripping Ring

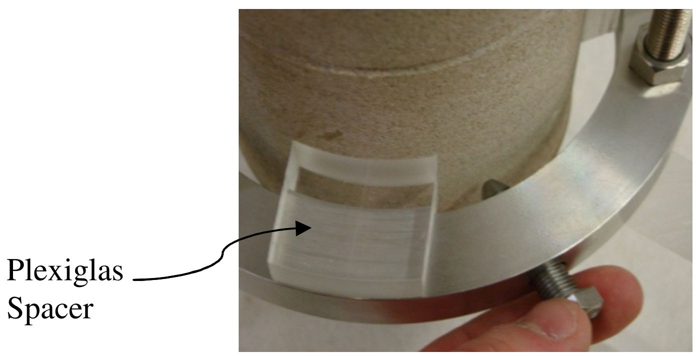

(b) Sharp Bolt Gripping Lower Ring to Sample

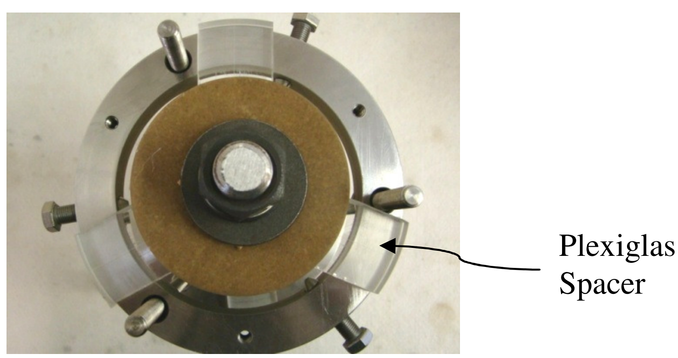

(c) Sharp Bolts Gripping Upper Ring to Sample

Figure 5.10 - Assembling Gripping Rings to Sample

Three holes in the upper ring and a set of six hexagonal nuts allow a fixed connection between the two gripping rings resulting in a fully gripped system. The system composed of the rings, the three bars and six bolts provided a full grip between the two halves of the sample. The central threaded rod system is removed and the fully gripped sample is placed in the water tank. The plexiglas water retainer is attached to the base of the reaction frame and the permeameter (connected to the pump, the pressure transducer and the de-airing pipe) is placed on the top surface of the sample. Throughout the preparation of the fractured samples for testing, plexiglas spacers that were machined to different shapes, were used for centering and alignment purposes (Figure 10).

The three Mitutoyo digimatic indicators (Model ID-N 543576, supplied by Yervant Industriel), with a measuring range of 12.7mm and a resolution of 0.001mm were held by plexiglas holders (Figure 5.11-a) and fixed on the upper stainless steel gripping ring with their “needle pins” touching the top of the threaded bars attached to the lower gripping ring. The three indicators provide signals to a Mitutoyo multiplexer (Model MIG 2B, Figure 5.11-b) which outputs it to the PC through a serial port. A Matlab program, was written (Appendix A) to convert the readings from the serial port pins to readable metric values.

(a) Mitutoyo Indicators with Plexiglas Holders

(b) Mitutoyo Multiplexer

Figure 5.11 - Hardware Used for Fracture Aperture Size Measurement

The six hexagonal nuts gripping the threaded bars to the upper gripping ring are now un-screwed, disconnecting the upper ring from the lower ring (Figure 5.12). Consequently, the bottom ring and the top ring are only connected to the lower sample half and the upper sample half respectively (Figure 5.12-b), and the three digital indicators can transmit the change in distance between the two gripping rings which corresponds to the change in the fracture aperture size. The indicators are set to zero and a small load is applied to provide a seal to de-air the system. The sample is now ready to be tested.

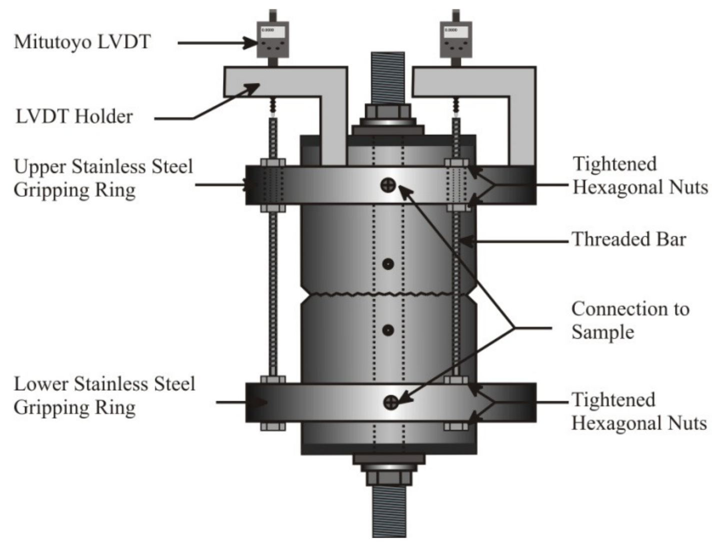

(a) Step 1

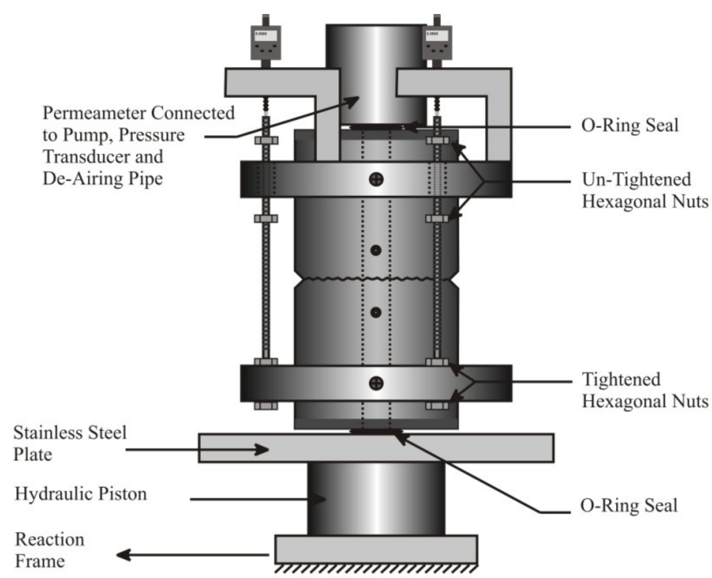

(b) Step 2

Figure 5.12 - Disconnecting the Two Parts of the Sample

Figure 5.13 shows the experimental configuration under the loading frame. The experimental procedure consists first, of applying a constant flow to the fractured sample until a steady inner pressure is recorded by the transducer. The load is then increased keeping the flow constant and the steady state pressure is recorded. This is repeated until reaching a load cycle peak and then the load is similarly incrementally decreased. Typically, three loading cycles were performed, and the change in fracture aperture size recorded at each steady state level reached.

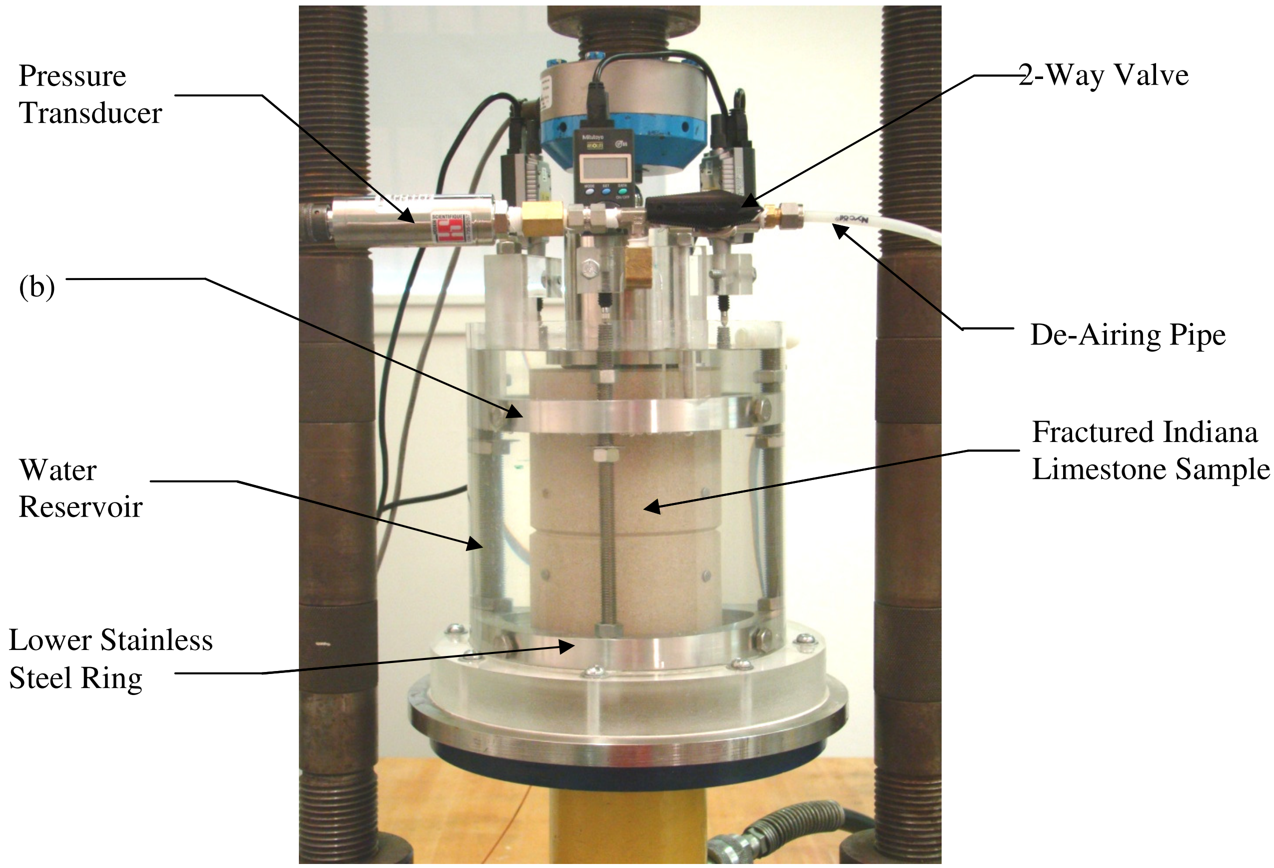

(a) Experimental Facility for Permeability Testing on Fractured Samples

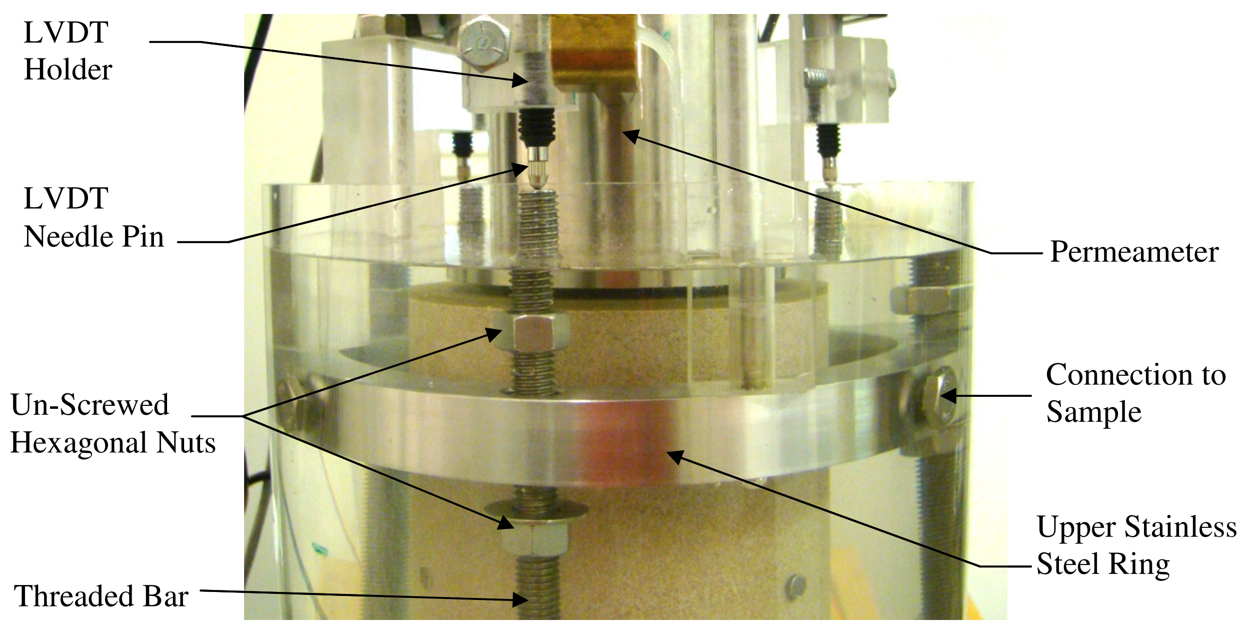

(b) Close-Up on Needle Pin in Contact with Threaded Bar

Figure 5.13 - Experimental Facility for Permeability Testing on Fractured Samples

5.4 - Sealing the Fractures and Testing the "Sealed-Fracture" Samples

The final stage of the research program involved sealing the fractures of the samples and re-testing the permeability of the sealed sample. A fast curing SIKA epoxy anchoring gel was used because of its relatively high viscosity; this prevented any sealing material from seeping in to the exposed surfaces of the sample which would form a barrier for the radial fluid flow. Figure 5.14 illustrates the steps followed to seal the fractures.

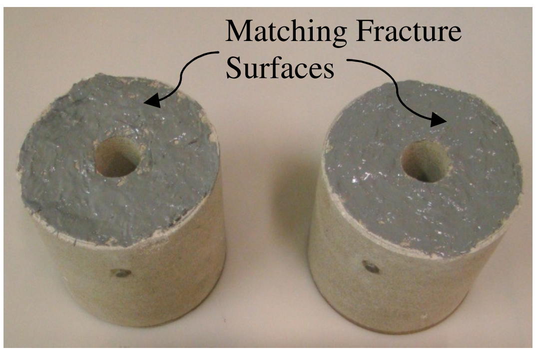

(a) The Two Fracture Faces Epoxy-Coated

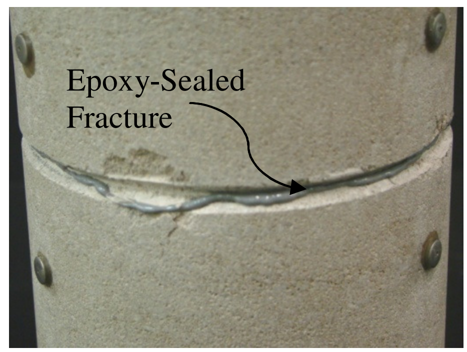

(b) Close-Up of the Sealed Fracture

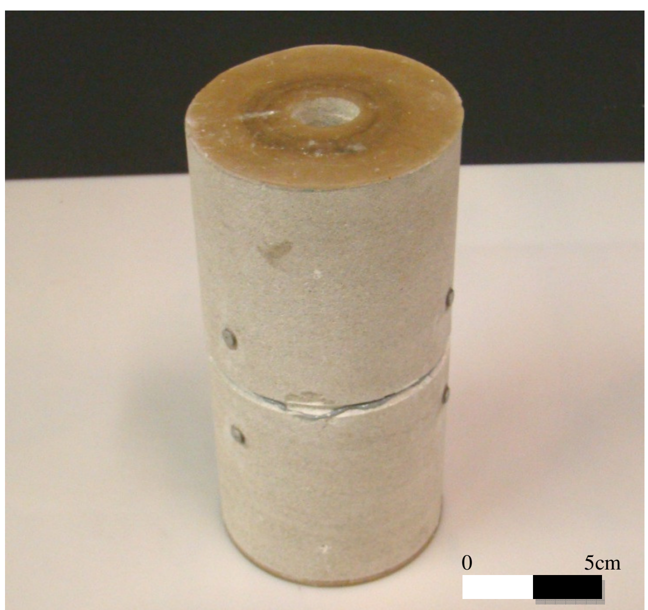

(c) "Fracture-Sealed" Sample Ready for Permeability Testing

Figure 5.14 - Sealing the Fractured Samples

Chapter 6 - Results and Discussion

This chapter presents the results obtained from the three sets of experiments performed to determine the permeability of intact, fractured and sealed Indiana Limestone samples.

6.1 - Intact Samples

Six intact Indiana Limestone samples were tested in the radial flow configuration to determine the permeability; as expected, there were variations in the results both within the sample group and within the separate samples, with a slightly more noticeable variation between results on each sample. Table 6.1 shows the resulting average permeability value of each sample determined using Eq.18. Flow rates of 2, 3 and 5mL/min were used during different experiments to confirm the repeatability of the experiments. Figure 6.1 shows the steady state pressures obtained in two typical experiments. As shown in Figure 6.1(b), some cavity pressure readings from the experiments showed the occurrence of one or more pressure changes in the form of spikes. These irregularities were considered to be noise caused by external voltaic influences on the data acquisition system and were disregarded in the calculation of the steady state pressure since the steady state values were virtually uninfluenced by these short duration changes.

Table 6.1 - Average Permeability Results for Intact Samples

Sample	Number of Experiments	Average Permeability $\times 10^{-15}$ m^2	Standard Deviation $\times 10^{-15}$
1	15	0.984	0.0953
2	12	1.869	0.0952
3	11	1.277	0.173
4	10	1.417	.0836
5	08	1.531	0.168
6	06	1.469	0.048

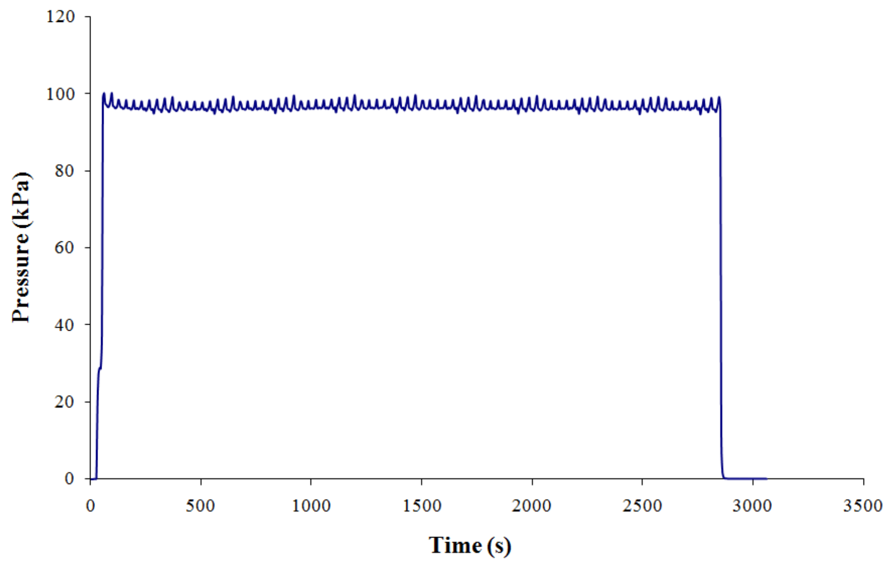

(a) Time-dependent evolution of cavity pressure for the 12th experiment on sample 1 subjected to a 5mL/min flow rate.

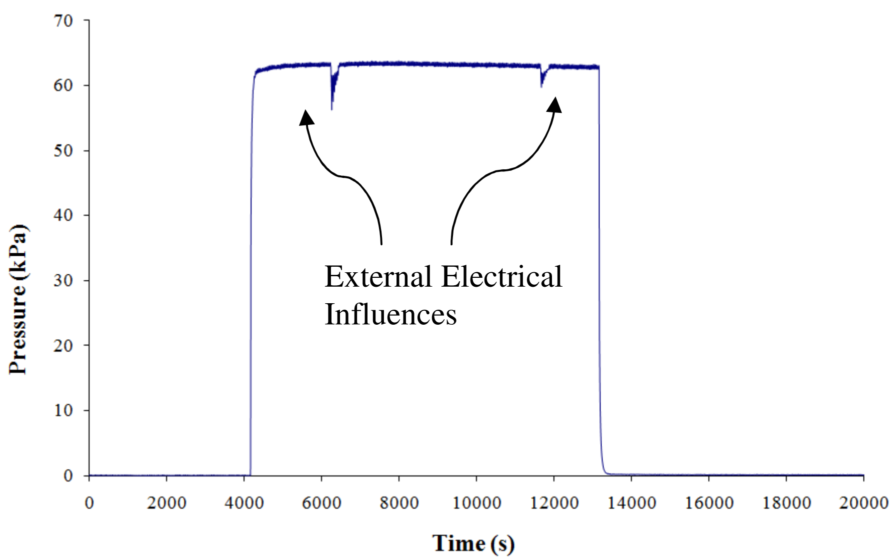

(b) Time-dependent evolution of cavity pressure for the 6th experiment on sample 4 subjected to a 5mL/min flow rate.

Figure 6.1 - Typical Time-Dependant Evolutions of Cavity Pressures

6.2 - Fractured Samples

Table 6.2 shows the initial fracture aperture sizes of the six samples, the load that was required to initiate the fracture and the torque at which the two Hex-nuts of the threaded rod assembly were tightened.

Table 6.2 - Initial Fracture Sizes and Fracturing Loads

Sample	Initial Fracture Aperture Size (mm)	Fracturing Load (kN)	Threaded Rod Assembly Torque (N-m)
1	0.12954	25	13.5
2	1.18618	30	4
3	0.32766	29	11
4	0.24892	28	13.5
5	0.24553	27	11
6	0.18203	26	13.5

The stress-dependant permeability results obtained from samples 4, 5 and 6 are reported in this section. The results obtained from the first three samples were considered erroneous due to handling accidents that caused the Fractured samples to separate, leading to unrealistically large aperture sizes with a large amount of debris trapped between the fractured surfaces or from an excessive splitting load applied after the occurrence of fracture propagation as was the case for sample 2. Every sample was subjected to three loading cycles where the peak load of each was increased at every cycle. Figures 6.2 to 6.4 show the loading cycles and the changes in fracture aperture size corresponding to each loading step for the three samples.

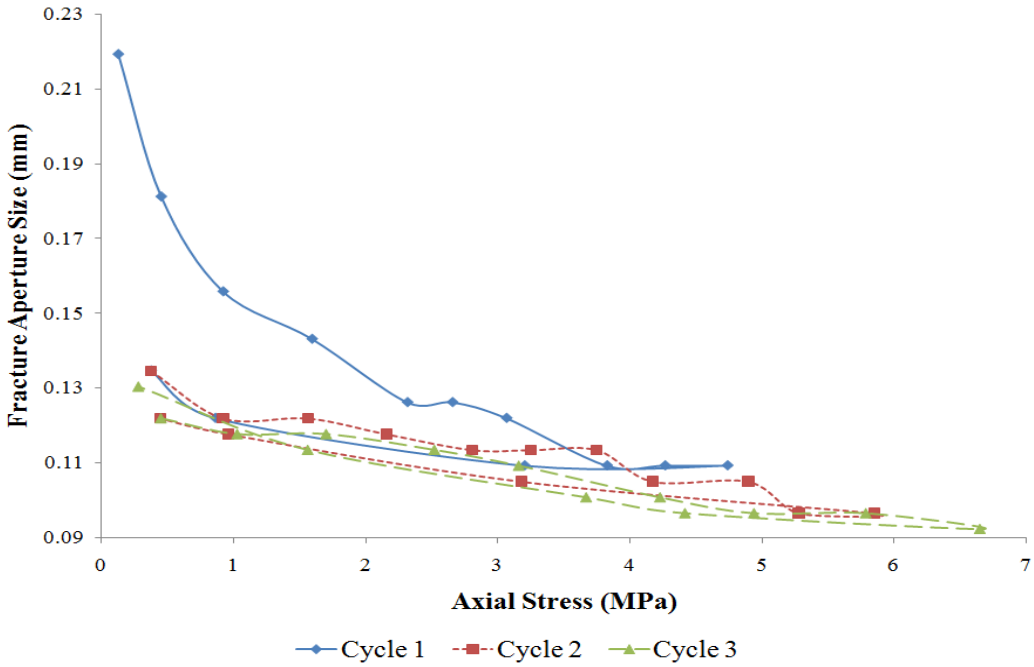

(a) Fracture Aperture Size Evolution with Cycled Axial Stress on Sample 4

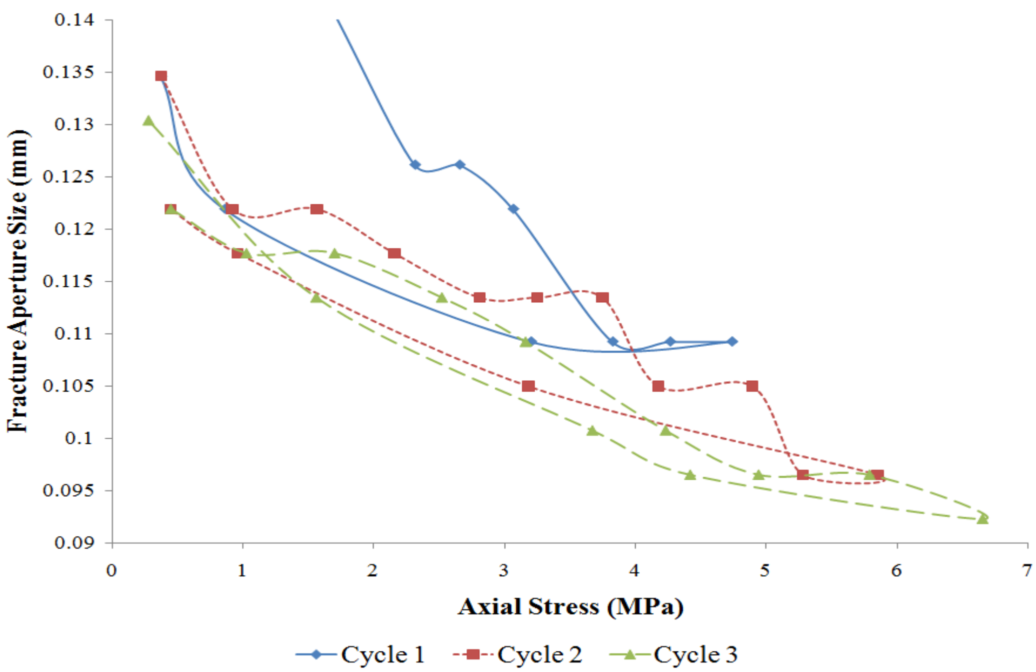

(b) Close-Up of Small Fracture Aperture Sizes

Figure 6.2 - Fracture Aperture Size Evolution with Cycled Axial Stress on Sample 4

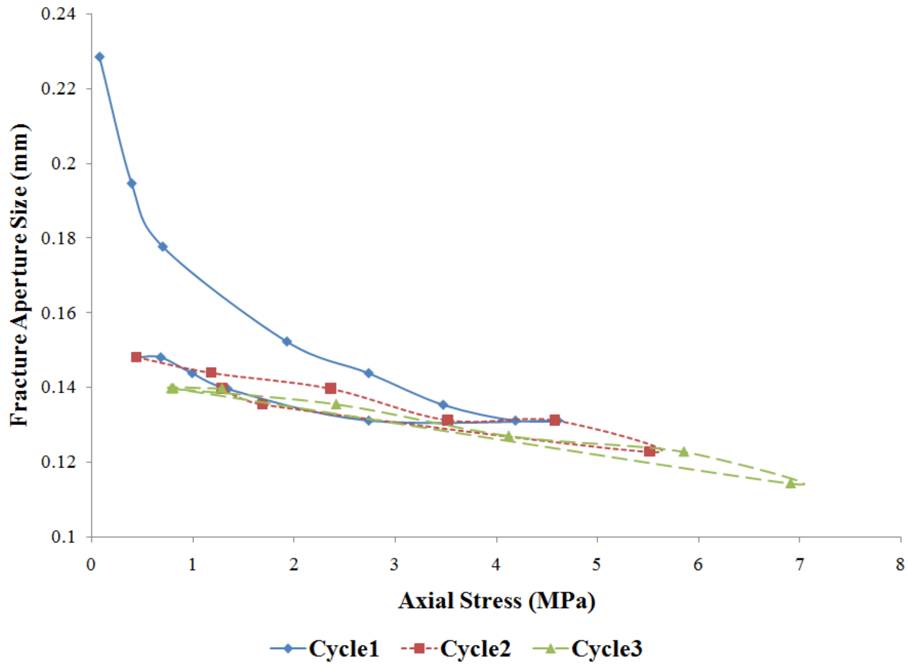

(a) Fracture Aperture Size Evolution with Cycled Axial Stress on Sample 5

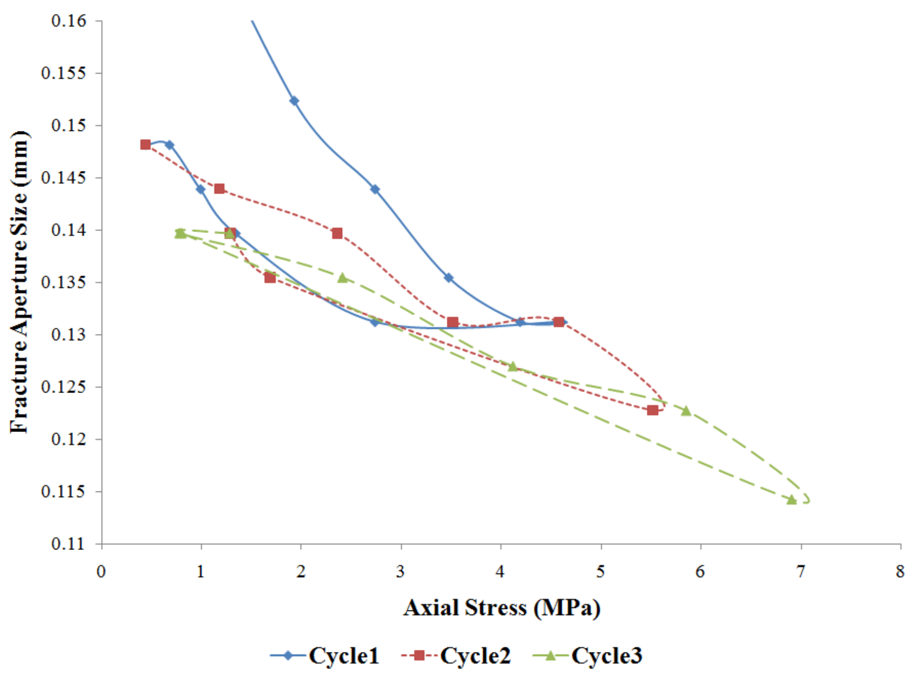

(b) Close-Up of Small Fracture Aperture Sizes

Figure 6.3 - Fracture Aperture Size Evolution with Cycled Axial Stress on Sample 5

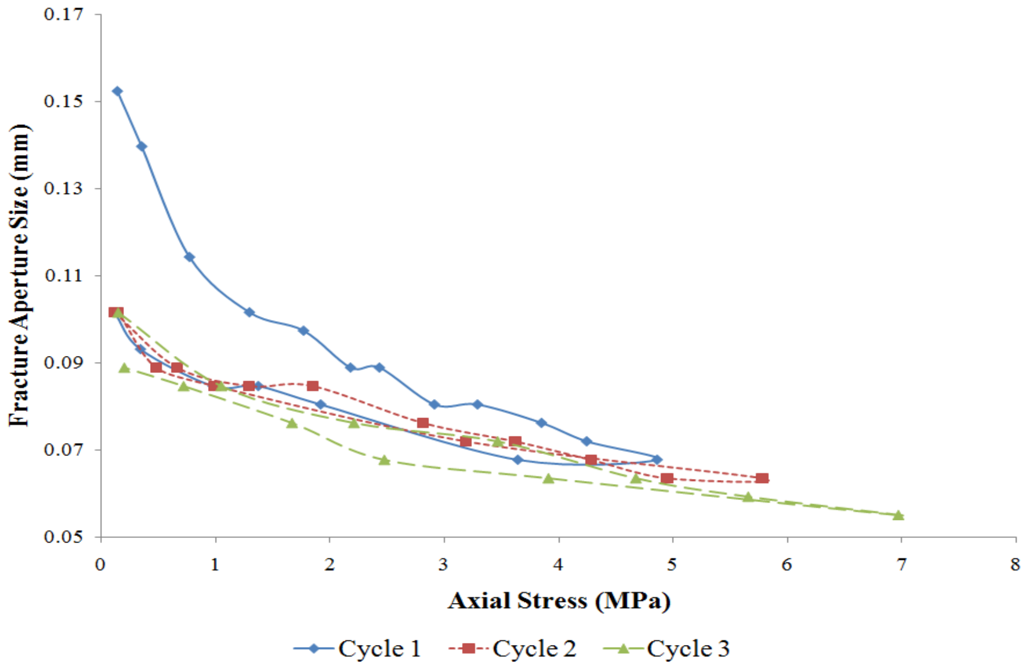

(a) Fracture Aperture Size Evolution with Cycled Axial Stress on Sample 6

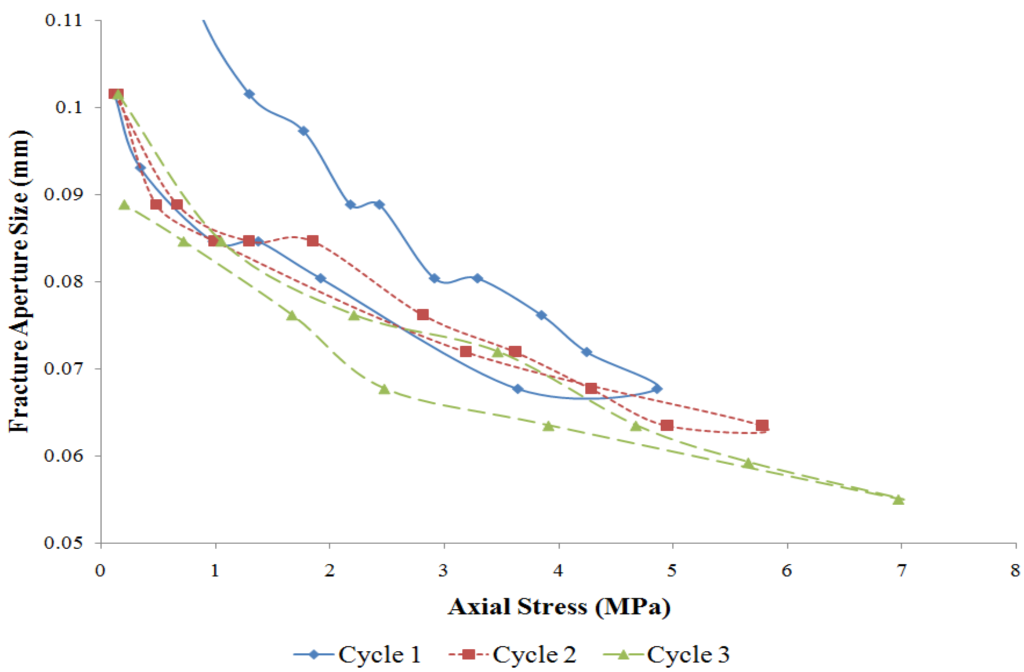

(b) Close-Up of Small Fracture Aperture Sizes

Figure 6.4 - Fracture Aperture Size Evolution with Cycled Axial Stress on Sample 6

The permeability of the fracture under a given level of axial stress is calculated from Eq.21, which relates the permeability of the hydraulic aperture and the intact permeability of the Indiana Limestone. Figures 6.5 to 6.7 illustrate the results obtained for samples 4 to 6 under 3 loading cycles. The duration of the loading steps varied from 15 minutes to approximately 90 minutes, depending on the level of stress applied. At lower stresses, the flow occurred almost exclusively in the relatively open fracture with minimal cavity pressure; steady state is consequently reached quickly. At higher stresses, the closure of the fracture results in a higher pressure build-up in the cavity and thus longer time to achieve a steady state. It can also be noticed from Figures 6.5(a), 6.6(a) and 6.7(a) that the largest reduction in permeability occurs at the first few (lower value) loading steps of the first cycle and that irreversible permeability reduction occurs at smaller proportions with every new cycle.

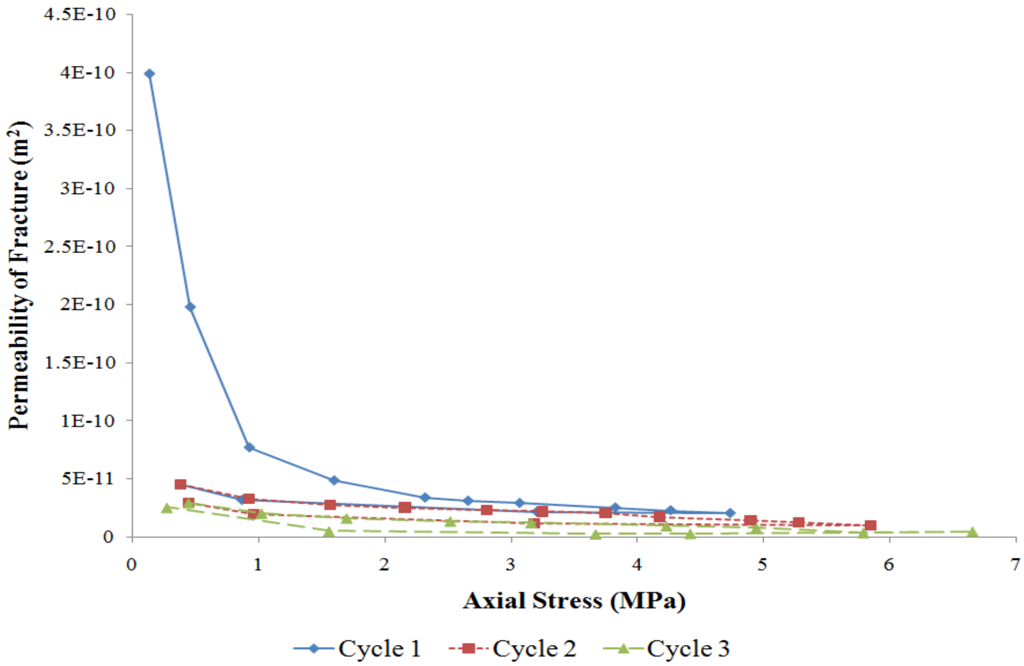

(a) Permeability Evolution with Cycled Axial Stress on Sample 4

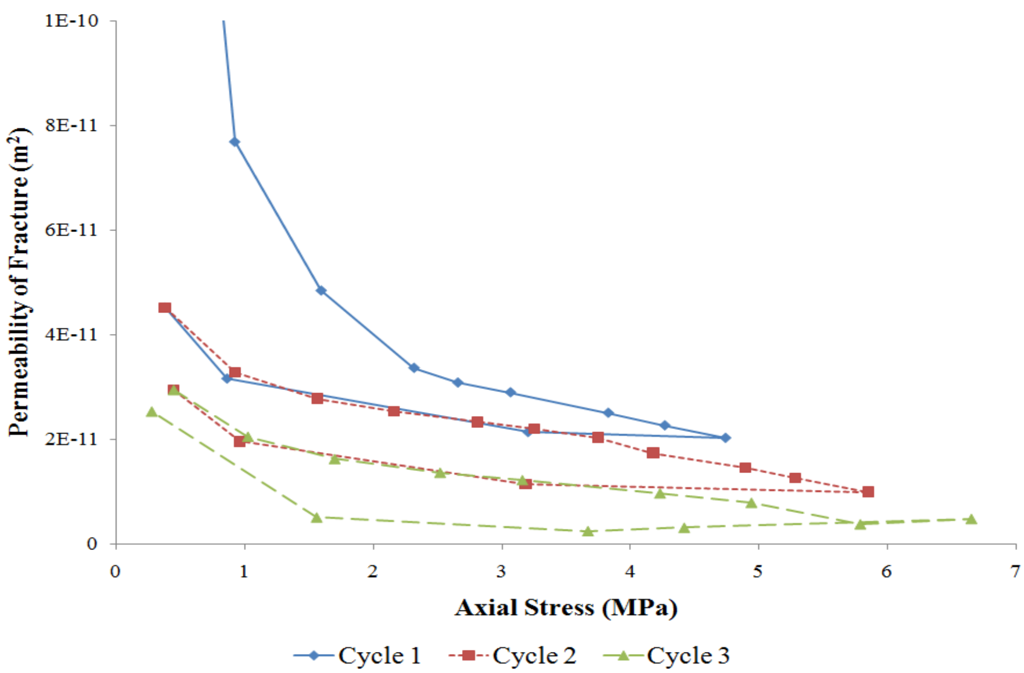

(b) Close-Up of Low Permeabilities

Figure 6.5 - Permeability Evolution with Cycled Axial Stress on Sample 4

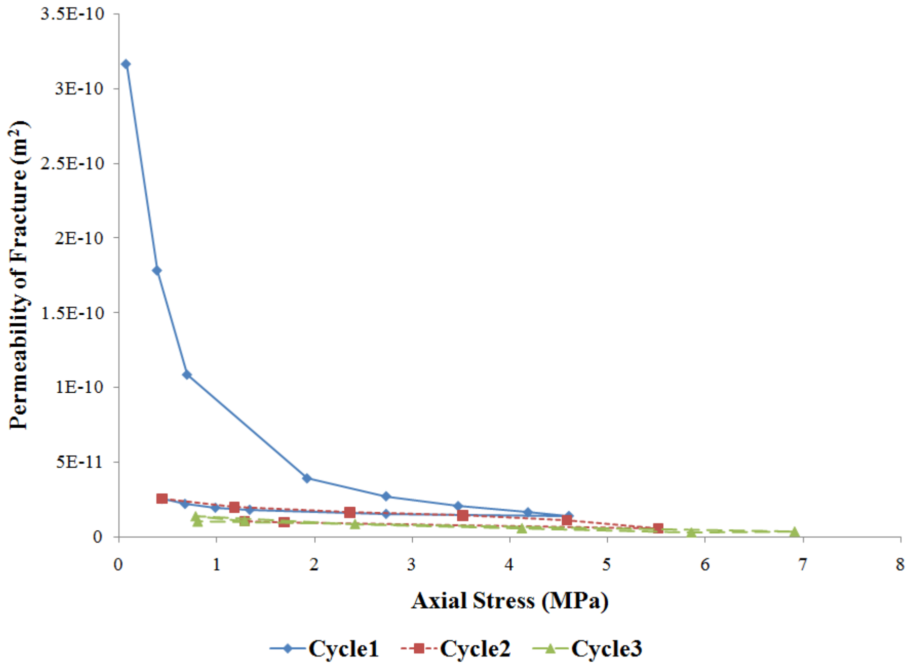

(a) Permeability Evolution with Cycled Axial Stress on Sample 5

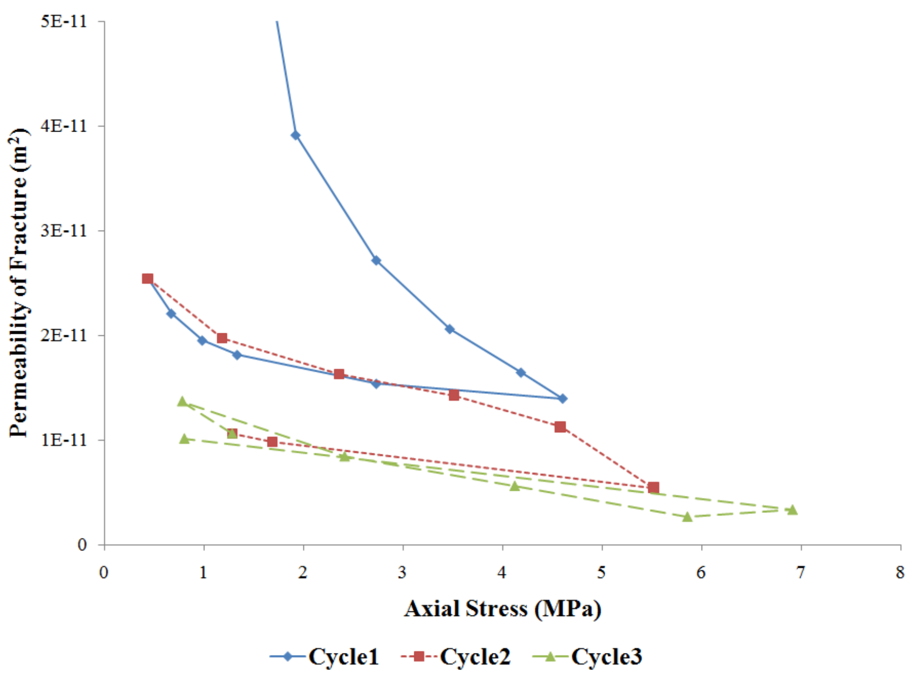

(b) Close-Up of Low Permeabilities

Figure 6.6 - Permeability Evolution with Cycled Axial Stress on Sample 5

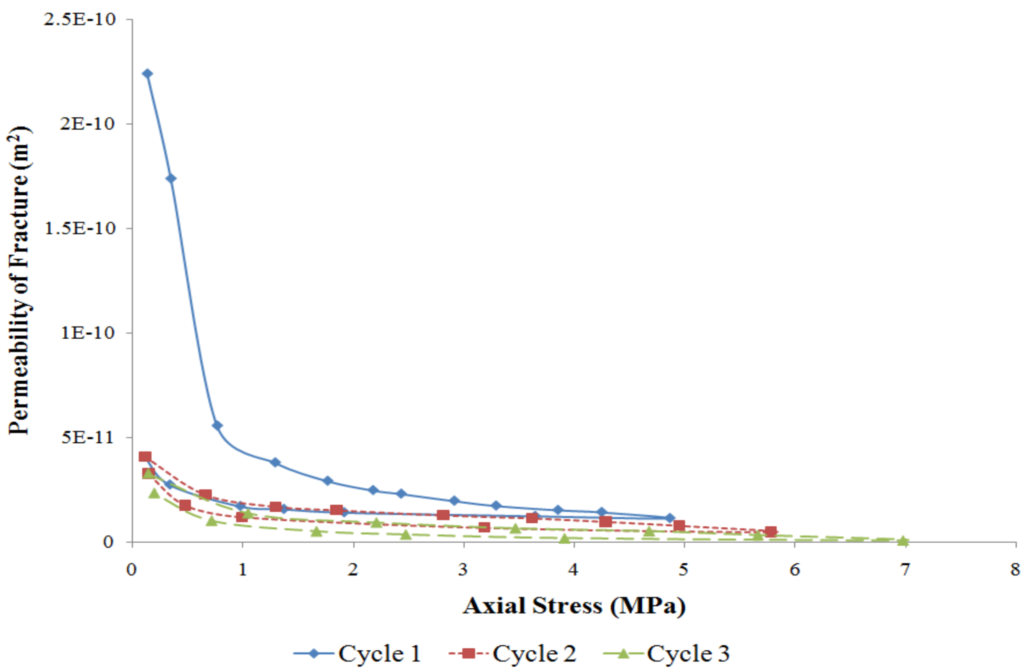

(a) Permeability Evolution with Cycled Axial Stress on Sample 6

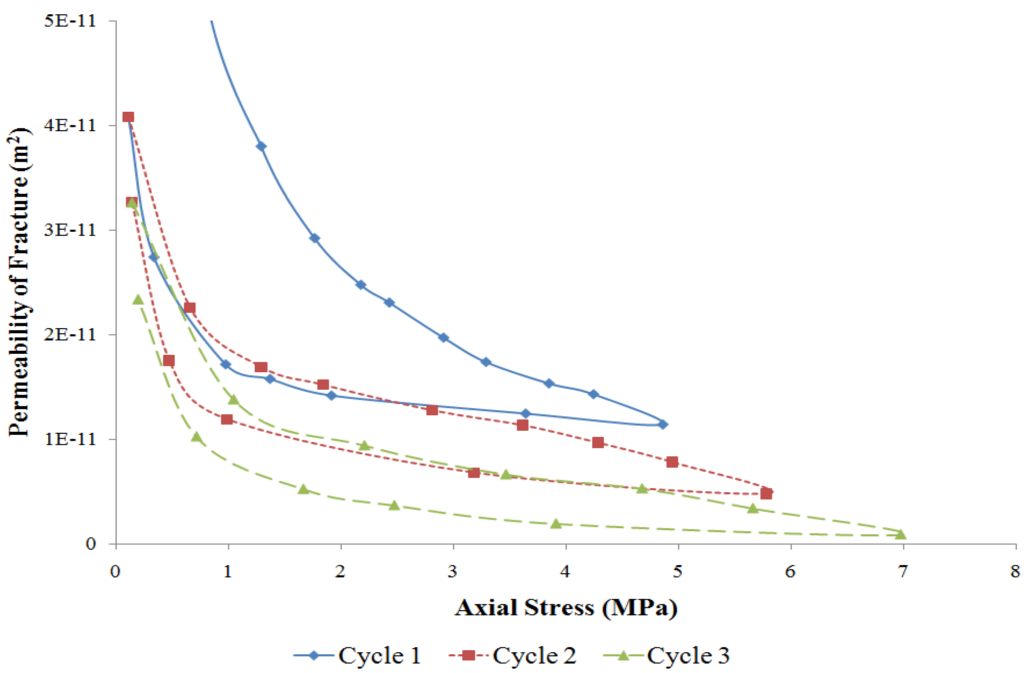

(b) Close-Up of Low Permeabilities

Figure 6.7 - Permeability Evolution with Cycled Axial Stress on Sample 6

6.3 - “Fracture-Sealed” Samples

Experiments were performed on the Indiana Limestone cylinders with fractures sealed as described in section 5.4 to measure the permeability of these remediated samples. Table 6.3 shows the average permeabilities obtained. The procedure followed to test these “Fracture-sealed” samples was identical to the procedure followed in testing the intact samples.

Table 6.3 - Average Permeability Results for “Fracture-Sealed” Samples

Sample	Number of Experiments	Average Permeability $\times 10^{-15}$ m^2	Standard Deviation $\times 10^{-15}$
1	8	0.412	0.0493
2	5	0.741	0.103
3	5	0.526	0.0239
4	3	0.512	0.512
5	4	1.019	0.0084
6	5	0.705	0.0285

6.4 - Analysis of Results and Sources of Error

The results from the permeability tests performed on the intact samples indicate variations in the results both within the sample group and within the separate samples with a slightly more noticeable variation between results on the separate samples. The variation in results within one sample, indicated by the standard deviation in Table 6.1, can be explained by the following: First, although the samples were subjected to vacuum pumping and then to saturation by normal pumping, an accurate measurement of porosity was not performed for each sample and thus the level of saturation was only assumed to have reached 100%. As shown by Selvadurai (2009), the degree of saturation can influence the attained steady state pressure. Second, the effect of the axial load applied to provide an efficient seal on the permeability of the limestone was neglected throughout the research. Glowacki (2008) shows clear instantaneous and permanent changes in the permeability of Indiana limestone due to confining pressure. The sealing pressure applied was kept constant at around 2MPa for all experiments on a single sample to prevent that source of variation, but a small yet constant change in the sealing pressure occurred. Temperature changes might also play a role since only an average value of the temperature for each experiment was used to determine the dynamic viscosity. The variations in permeability results within the separate samples were, in fact expected even though Indiana Limestone is considered to be relatively homogenous (ILIA, 1998),

Table 2.1 shows that certain results for permeability have much greater variations, particularly within one sample (Selvadurai and Selvadurai, 2009). The results obtained in this research indicate a highly homogenous type of Indiana Limestone. Anisotropic properties were not detected by naked eye, and all samples were cored in the same direction to avoid any variations caused by possibly existing anisotropic properties. The range of the permeability obtained in this research 0.9×10^{-15} m^2 to 1.9×10^{-15} m^2 is considered usable for applications involving highly homogenous Indiana Limestone.

The results obtained for the fractured specimens were considered satisfactory when compared to those reported by Selvadurai (2008) who performed a similar test on a large cylindrical granite sample with a cylindrical cavity. The hysteresis effect (Figures 6.5 to

6.7) is explained by the mismatches in the surfaces of the fracture which creates additional fluid pathways; these mismatches drastically decrease following the first loading cycle because the two surfaces of the fracture become well aligned which minimizes the fluid pathways. That effect decreases after several loading cycles because the deformation of the fracture becomes more elastic after the alignment of the fracture surfaces (National Research Council, 1996). The values obtained by performing these tests on the Indiana Limestone samples are quite consistent but some errors can be introduced even in these tests. The level of saturation, the temperature and the loads applied for sealing the cavity can explain possible errors in the tests on fractured samples, but the most dominant source of error involves the fracture itself. From a theoretical point of view, the permeability of the fracture was determined using the parallel plate model; however, in most cases, when splitting the Indiana Limestone samples the fractures propagated slightly beyond the grooves and therefore do not correspond closely to the parallel plate model. Furthermore, a standardized test or procedure for fracturing cylindrical stone samples and determining the initial fracture aperture size does not exist and the effect of water, temperature and other factors on the epoxy-glued Demec points (Figure 5.4) used for measuring the initial fracture aperture size is unknown. Some aspects of the results, such as the order of magnitude drop of permeability after the occurrence of the fracture and the pattern followed by the permeability values with quasi-cycled loading can be pertinent to understanding the hydraulic behavior of fractures subjected to real life stresses.

The results obtained from the "fracture-sealed" samples indicate a drop of less than 1 order of magnitude in the permeability of all the samples. The most probable reason for that would be the excessively large stresses (7MPa) applied on the fractured samples which would cause permanent effects on the permeability of the intact Indiana Limestone. Furthermore, the reactivity of the type of sealant used with Indiana Limestone was never tested which could also explain that drop in permeability; this is unlikely though due to the relatively short period of time spent between sealing the fracture and testing the sample.

Chapter 7 - Conclusions and Recommendations

The hydraulic behavior of fractures has been part of several investigations; however, this research was innovative in the evaluation of the permeability and hydraulic behavior of fractures in Indiana Limestone and the application of quasi-cycled stresses. The relatively recent and serious move towards the storage of toxic waste in deep underground repositories requires such an understanding of the permeability behavior of the rock in particular under different external effects. The highest permeabilities (2.5×10^{-10} m^2 to 4×10^{-10} m^2) were observed in the fractured samples at the minimum level of stress applied (beginning of first cycle). The experimental investigation shows an irreversible decrease in permeability of around one order of magnitude after three loading cycles. A further decrease in permeability can thus be expected with additional loading cycles but at a lower rate of decrease with each cycle.

The highest stress applied on the fractures was 7MPa and the corresponding permeability was still four orders of magnitude higher than the permeability of the intact samples; this indicates that, in order to completely close the fracture, very high stresses need to be applied.

In future work, it would be useful to conduct similar studies on different materials and/or to apply a wider array of stress combinations and cycles, such as confinement pressure in addition to axial stresses. This would be a non-trivial task since the application of confining pressures is more suited for axial flow tests rather than radial flow tests due to some experimental setup restrictions.

References

Areias, L. C., and Lo, K. Y., 2006, Laboratory measurement of hydraulic conductivity of rocks from Lakeview borehole: *Proceedings of the International Symposium of the International Society for Rock Mechanics, Liège, Belgium,* p. 115-120.

Bandis, S., Lumsden, A., and Barton, N., 1983, Fundamentals of rock joint deformation: *International journal of rock mechanics and mining sciences*, v. 20, p. 249-268.

Bandis, S., Makurat, A., and Vik, G., 1986, Predicted and measured hydraulic conductivity of rock joints: *Publikasjon- Norges Geotekniske Institutt*, p. 1-11.

Barton, N., and Choubey, V., 1977, The shear strength of rock joints in theory and practice: *Rock Mechanics and Rock Engineering*, v. 10, p. 1-54.

Bencsik, M., and Ramanathan, C., 2001, Method for measuring local hydraulic permeability using magnetic resonance imaging: *Physical Review Series E*, v. 63, p. 65302-65302.

Bernabe, Y., 1986, The effective pressure law for permeability in Chelmsford Granite and Barre Granite: *International Journal of Rock Mechanics and Mining Sciences and Geomechanics Abstracts*, v. 23, p. 267-275.

Bernabe, Y., Brace, W. F., and Evans, B., 1982, Permeability, porosity and pore geometry of hot-pressed calcite: *Mechanics of Materials*, v. 1, p. 173-183.

Boulon, M., Selvadurai, A., Benjelloun, H., and Feuga, B., 1993, Influence of rock joint degradation on hydraulic conductivity: *International journal of rock mechanics and mining sciences*, v. 30, p. 1311-1317.

Bourbie, T., and Walls, J., 1982, Pulse decay permeability: analytical solution and experimental test: *Society of Petroleum Engineering, AIME, Pap*, v. 22, p. 719-721.

Brace, W. F., Walsh, J. B., and Frangos, W. T., 1968, Permeability of granite under high pressure: *Journal of Geophysical Research*, v. 73, p. 2225-2236.

Bredehoeft, J., and Papadopulos, S., 1980, A method for determining the hydraulic properties of tight formations: *Water Resources Research*, v. 16.

Carnaffan, P., 1994, *An Experimental Technique for Determining the Permeability of Rock, Concrete and Cement Grout. M. Eng*, Thesis, Department of Civil and Environmental Engineering, Carleton University, Ottawa, ON.

Darcy, H., 1856, Les fontaines publiques de la ville de Dijon: *Dalmont, Paris*, v. 647.

Daw, G. P., 1971, A modified Hoek-Franklin triaxial cell for rock permeability measurements: *Géotechnique*, v. 21, p. 89.

Engelder, T., and Scholz, C., 1981, Fluid flow along very smooth joints at effective pressures up to 200 megapascals: *Mechanical Behaviour of Crustal Rocks, Amer. Geoph. Union Mono*, v. 24, p. 147-152.

Gale, J., 1982, Assessing the permeability characteristics of fractured rock: *Geological Society of America Special Paper*, v. 189, p. 163-181.

Glowacki, A., 2008, *The Permeability Hysterisis of Indiana Limestone During Isotropic Compression. M. Eng*, Thesis, Department of Civil and Applied Mechanics, McGill University, Montreal, QC.

Haimson, B., and Doe, T., 1983, State of stress, permeability, and fractures in the Precambrian granite of northern Illinois: *Journal of Geophysical Research*, v. 88, p. 7355-7371.

Heystee, R., and Roegiers, J. C., 1981, The effect of stress on the primary permeability of rock cores-a facet of hydraulic fracturing: *Canadian Geotechnical Journal*, v. 21, p. 257-261.

Hoek, E., and Franklin, J. A., 1967, A simple triaxial cell for field or laboratory testing of rock: *Transactions of the Institution of Mining and Metallurgy*, v. 77, A22-26.

ILIA, 1998, *Indiana Limestone Handbook*: Indiana Limestone Institute of America Inc, Bedford, Indiana, USA.

Iwai, K., 1976, *Fundamental Studies of Fluid Flow Through a Single Fracture, P.h.D*, Thesis, Univ. of California, Berkeley

Jaeger, C., 1972, *Rock Mechanics and Engineering*, Cambridge University Press, Cambridge.

Kranz, R., Frankel, A., Engelder, T., and Scholz, C., 1979, The permeability of whole and jointed Barre Granite: *International Journal of Rock Mechanics and Mining Sciences and Geomechanics Abstracts*, v. 16, p. 225-344.

Lafhaj, Z., Richard, G., Kaczmarek, M., and Skoczylas, F., 2007, Experimental determination of intrinsic permeability of limestone and concrete: Comparison between in situ and laboratory results: *Building and Environment*, v. 42, p. 3042-3050.

Lockner, D., Hickman, S., Kuksenko, V., Ponomarev, A., Sidorin, A., Byerlee, J., and Khakaev, B., 1991, Laboratory-determined permeability of cores from the Kola superdeep well, USSR: *Geophysical Research Letters*, v. 18, p. 881-4.

Londe, P., and Sabarly, F., 1966, La distribution des permeabilites dans la fondation des barrages voutes en fonction du champ de contrainte: *International Society of Rock Mechanics*, v. 2, p. 517-521.

Makurat, A., Barton, N., Rad, N., and Bandis, S., 1990, Joint conductivity variation due to normal and shear deformation: *Rock Joints. Balkema, Rotterdam*, p. 535-540.

Mattar, P., and Selvadurai, A. P. S., 2009, Radial flow permeability testing of Indiana Limestone: *Proceedings of the 3rd CANUS Rock Mechanics Symposium, May 2009*, (Ed: M.Diederichs and G. Grasselli), Toronto, Ontario p. Paper-4119: 1-7.

Mayer, A., 1963, Recent work in rock mechanics: *Géotechnique*, v. 13, p. 99-120.

Morrow, C., and Byerlee, J., 1988, Permeability of rock samples from Cajon Pass, California: *Geophysical Research Letters*, v. 15, p. 1033-6.

National Research Council, 1996, *Rock Fractures and Fluid Flow: Contemporary Understanding and Applications*, National Academy Press.

Nguyen, T. S., and Selvadurai, A. P. S., 1998, Model for coupled mechanical and hydraulic behaviour of a rock joint: *International Journal for Numerical and Analytical Methods in Geomechanics*, v. 22, p. 29-48.

Olsen, H. W., 1966, Darcy's Law in saturated Kaolinite: *Water Resources Research*, v. 2.

Olsen, H. W., Nichols, R. W., and Rice, T. L., 1985, Low gradient permeability measurements in a triaxial system: *Géotechnique*, v. 35, p. 145-157.

Pyrak-Nolte, L., and Morris, J., 2000, Single fractures under normal stress: The relation between fracture specific stiffness and fluid flow: *International journal of rock mechanics and mining sciences*, v. 37, p. 245-262.

Raven, K., and Gale, J., 1985, Water flow in a natural rock fracture as a function of stress and sample size: *International journal of rock mechanics and mining sciences*, v. 22, p. 251-261.

Selvadurai, A., 2000, *Partial Differential Equations in Mechanics: The biharmonic equation, Poisson's equation*, v. 1, Springer Verlag.

Selvadurai, A. P. S., 2008, Normal stress-induced permeability reduction of a fracture in a large granite cylinder: *Proceedings of GEOPROC 2008, International Conference on Coupled THMC Processes in Porous Media*,Lille, France p. 211 - 218.

Selvadurai, A. P. S., 2009, Influence of residual hydraulic gradients on decay curves for one-dimensional hydraulic pulse tests: *Geophysical Journal International*, v. 177, p. 1357-1365.

Selvadurai, A. P. S., Boulon, M. J., and Nguyen, T. S., 2005, The Permeability of an Intact Granite: *Pure and Applied Geophysics*, v. 162, p. 373-407.

Selvadurai, A. P. S., and Carnaffan, P., 1997, A transient pressure pulse method for the measurement of permeability of a cement grout: *Canadian Journal of Civil Engineering*, v. 24, p. 489-502.

Selvadurai, A. P. S., and Glowacki, A., 2008, Permeability hysterisis of limestone during isotropic compression: *Ground Water*, v. 46, p. 113-119.

Selvadurai, A. P. S., and Yu, Q., 2005, Mechanics of a discontinuity in a geomaterial: *Computers and Geotechnics*, v. 32, p. 92-106.

Selvadurai, P. A., and Selvadurai, A. P. S., 2007, On cavity flow permeability testing of a sandstone: *Ground Water*, v. 45, p. 93-97.

Selvadurai, P. A., and Selvadurai, A. P. S., 2009, On the surface permeability of Indiana Limestone: *Proceedings of the 3rd CANUS Rock Mechanics Symposium, May 2009*, (Ed: M.Diederichs and G. Grasselli), Toronto, Ontario p. Paper-4118: 1-9.

Snow, D., 1965, *A Parallel Plate Model of Fracture Permeable Media, Ph. D*, Thesis. Berkeley: University of California, Berkeley.

Song, I., Elphick, S. C., Main, I. G., Ngwenya, B. T., Odling, N. W., and Smyth, N. F., 2004, One-dimensional fluid diffusion induced by constant-rate flow injection: theoretical analysis and application to the determination of fluid permeability and specific storage of a cored rock sample: *Journal of Geophysical Research*, v. 109, p. 13 pp.

Song, I., and Renner, J., 2006, Linear pressurization method for determining hydraulic permeability and specific storage of a rock sample: *Geophysical Journal International*, v. 164, p. 685-96.

Stagg, K. G., and ZienZiewicz, O. C., 1968, *Rock Mechanics in Engineering Practice*, John Wiley and Sons, New York.

Suri, P., Azeemuddin, M., Zaman, M., Kukreti, A. R., and Roegiers, J. C., 1997, Stress-dependent permeability measurement using the oscillating pulse technique: *Journal of Petroleum Science and Engineering*, v. 17, p. 247-264.

Tidwell, V., and Wilson, J., 1997, Laboratory method for investigating permeability upscaling: *Water Resources Research*, v. 33.

Trimmer, D., Bonner, B., Heard, H., and Duba, A., 1980, Effect of pressure and stress on water transport in intact and fractured gabbro and granite: *Journal of Geophysical Research-Solid Earth*, v. 85, p. 7059-7071.

Walsh, J., 1981, Effect of pore pressure and confining pressure on fracture permeability: *International journal of rock mechanics and mining sciences*, v. 18, p. 429-435.

Zeng, Z., and Grigg, R., 2006, A criterion for non-Darcy flow in porous media: *Transport in Porous Media*, v. 63, p. 57-69.

Appendix A – Matlab Code for Mitutoyo LVDTs

Function 1

```
function sp = connectDevice(port);
  sp = serial(port);
  set(sp, 'Terminator', 'CR');
  set(sp, 'BaudRate', 4800);
  set(sp, 'StopBits', 1);
  set(sp, 'DataBits', 8);
  set(sp, 'Parity', 'none');
  set(sp, 'FlowControl', 'none');
   fopen(sp);
```

Function 2

```
function d = readGage (sp, gage)
 fprintf (sp, ' % d \n', gage);
  datastring = fscanf (sp);
fprintf (' Gage % d:  % s \n', gage, datastring);
 d = datastring (4:10);
```

Program

```
delay = 1;
port = 'COM1';
sp = connectDevice(port);
t = clock;
year = t(1);
month = t(2);
day = t(3);
hour = t(4);
minutes = t(5);
seconds = t(6);
 filename = sprintf('results-%d-%d-%d-%d.txt', month, day, hour, minutes);
 fprintf('Print to file: $filename\n');
while (1)
  t = clock;
  year = t(1);
  month = t(2);
  day = t(3);
  hour = t(4);
  minutes = t(5);
  seconds = t(6);
  s = sprintf('%d-%d-%d-%d-%.0f,', month, day, hour, minutes, seconds);
  for gage=1:2
    d = readGage(sp, gage);
    s = sprintf('%s %s, ', s, d);
  end
```

```
  fid = fopen(filename, 'a');
  fprintf(fid, '%s\n', s);
  fclose(fid);
  pause(delay);
end
fclose(sp);
```